UNIVERSITY OF CALIFORNIA, SAN DIEGO

Temperature Effects on Pullout of Woven Geotextiles from Unsaturated Silt

A Thesis submitted in partial satisfaction of the

requirements for the degree Master of Science

in

Structural Engineering

by

Bernardo Ambriz

Committee in charge:

Professor John S. McCartney, Chair
Professor Ahmed M. Elgamal
Professor Ingrid Tomac

2018

The Thesis of Bernardo Ambriz is approved, and it is acceptable in quality and form for publication on microfilm and electronically:

_____

_____

_____

Chair

University of California, San Diego

2018

TABLE OF CONTENTS

SIGNATURE PAGE iii
TABLE OF CONTENTS iv
LIST OF FIGURES vi
LIST OF TABLES viii
ACKNOWLEDGMENTS ix
ABSTRACT OF THE THESIS xi
Chapter 1 - Introduction 1
1.1 Motivation 1
1.2 Objectives 4
1.3 Approach 5
1.4 Organization 5
Chapter 2 - Literature Review 7
2.1 Effective Stress in Unsaturated Soils 7
2.2 Thermal Effects on Unsaturated Soils 9
2.3 Geosynthetic Tensile Strength and Confining Stress Effects 15
2.4 Thermal Effects on Geosynthetic Stiffness 16
2.5 Soil-Geosynthetic Interaction in Pullout Tests 17
Chapter 3 - Materials and Methods 21
3.1 Testing Apparatus 21
3.2 Materials 24
3.3 Experimental Procedures 27
Chapter 4 - Results 29
4.1 Overview of Testing Program 29
4.2 Testing Series 1 - Pullout Tests on PP Geotextiles 31
4.2.1 Heating Phase 31
4.2.2 Pullout Phase 35
4.3 Testing Series 2 - Pullout Tests on PET Geotextiles 35
4.3.1 Heating Phase 35
4.3.2 Pullout Phase 40
Chapter 5 - Analysis 42
5.1 Synthesis of Experimental Results 42
5.2 Effective Stress Analysis of Pullout Resistance 43

Chapter 6 - Conclusion 49
6.1 Conclusion 49
6.2 Recommendations for Future Research 50
References 51

LIST OF FIGURES

Figure 1.1 Simplified elevation of typical configuration of an MSE Wall: (a) Conventional MSE wall; (b) Thermally-active MSE wall showing geosynthetic heat exchangers in the reinforced backfill soil ……. 3

Figure 2.1 Numerical model of earthen embankment with horizontal heat exchanger: (a) Temperature profiles; (b) Change in degree of saturation within 2 m of central heat exchanger (from Coccia and McCartney 2013) …….. 11

Figure 2.2 Specific volume against temperature at different matric suctions (from Uchaipichat and Khalili 2009): (a) Tests under a net stress of 50 kPa (higher OCR); (b) Tests under a net stress of 200kPa (lower OCR) …… 12

Figure 2.3 Loading collapse (LC) curves at different temperatures in terms of: (a) Effective Preconsolidation Stress; (b) Net Preconsolidation Stress (from Uchaipichat and Khalili 2009)……. 13

Figure 2.4 Temperature- and suction-controlled conventional compression shear tests: (a) initial mean effective stress of 50 kPa; (b) initial mean effective stress of 100 kPa; (c) initial mean effective stress of 300 kPa (from Uchaipichat and Khalili 2009) ……. 14

Figure 2.5 Peak shear strengths from temperature- and suction-controlled conventional shear tests: (a) initial mean effective stress of 50 kPa; (b) initial mean effective stress of 100 kPa; (c) initial mean effective stress of 300 kPa…… 15

Figure 2.6 Load-strain relationship for geotextile under confined and unconfined conditions (from McGown et al. 1982) ……. 16

Figure 2.7 Stress-strain behavior of geosynthetics in thermally active conditions: (a) deflection as a function of P_{ult} applied; (b) deflection as a function of time (from Stewart et al. 2013) …… 17

Figure 2.8 Plan view of pullout box meeting the requirements of ASTM D6706 (from Carpenter et al. 2015) ……..... 18

Figure 2.9 Vertical pressure ratio (measured/applied stress) as a function of distance from the side wall (from Farrag et al. 1993) …… 19

Figure 2.10 Displacement-controlled pullout load with varying length of bearing sleeve in pullout box opening (from Chang et al. 2000) …….. 20

Figure 2.11 Normalized pullout force as a function of soil cover depth (Brand and Duffy 1987)……. 20

Figure 3.1 Pullout device: (a) Elevation view schematic; (b) Plan view schematic; (c) Picture showing the different components …… 22

Figure 3.2 Inside of the pullout device: (a) Elevation view schematic; (b) Copper heat exchangers embedded into Delrin plates; (c) Dielectric sensor (temperature and volumetric water content) to be embedded in the soil; (d) Geosynthetic installation; (e) Upper loading plate with copper heat exchangers …… 24

Figure 3.3 Drying path soil-water retention curve and suction stress characteristic curve for Bonny silt under different temperatures predicted using Grant and Salehzadeh (1996) and Lu et al. (2010), respectively……... 25

Figure 4.1 Typical consolidation data and applied vertical stress during the loading period of 24 hours ……. 30

Figure 4.2 Thermo-hydraulic response of the soil for the specimens without a seating load: …. 33

Figure 4.3 Monotonic pullout profile views of soil properties: (a) temperature distribution along the specimen; (b) change in volumetric water contents from dielectric from the start of heating phase to pullout; (c) average volumetric water content from sampling after test ……. 34

Figure 4.4 Monotonic pullout results: (a) Load versus time and displacement versus time; (b) force versus displacement (P-d) curve ……... 35

Figure 4.5 Thermal creep under a seating pullout load of 1.43 kN/m …… 36

Figure 4.6 Thermo-hydraulic response of the soil for the specimens with a seating load:……... 38

Figure 4.7 Seated load with monotonic pullout profile views of soil properties: ……. 39

Figure 4.8 Room temperature pullout results for PET geotextile to determine seating pullout load…… 40

Figure 4.9 Seated load with monotonic pullout results: (a) load versus time and displacement versus time; (b) force versus displacement (P-d) curve ……. 41

Figure 5.1 Hypothetical water movement within the specimen during the heating phase ……... 43

Figure 5.2 Definition of the thermal softening parameter from the temperature- and suction-controlled triaxial compression shear tests of Uchaipichat and Khalili (2009) ……. 45

Figure 5.3 Comparison of the measured and predicted pullout resistances for the tests on PP geotextiles without a seating load: (a) pullout resistance versus temperature; (b) pullout resistance versus effective stress ……... 46

Figure 5.4 Comparison of the measured and predicted pullout resistances for the tests on PET geotextiles with a seating load: (a) pullout resistance versus temperature; (b) pullout resistance versus effective stress ……... 47

LIST OF TABLES

Table 3.1 Geotechnical properties of Bonny silt and initial conditions used in the experiments……... 26

Table 4.1 Summary of initial soil conditions and geosynthetic specifications ……. 31

Table 5.1 Percent errors between measured and prediction models of pullout resistances for PP and PET geotextiles …….. 48

ACKNOWLEDGMENTS

First and foremost, I would like to thank my thesis advisor, Professor John S. McCartney, for his guidance, support, advice, and help throughout the entirely of this journey. I am truly lucky and honored to have had such a great advisor. I was glad to always feel welcomed in approaching him with questions with my research project as well as all the opportunities he presented to me throughout my undergraduate and graduate studies, from helping out other students by being his teaching assistant to assisting other researching students in their projects. I will always appreciate everything he has done for me in my studies and all the doors he has opened up for my future.

I would also like to thank my committee members, Professor Ingrid Tomac and Professor Ahmed Elgamal, for their time and comments on my research.

My sincere gratitude also goes out to all my friends and fellow students at UCSD for their continuous help, support and friendship. I would particularly like to thank Woongju Mun for providing me the first set of test results along with his willingness to help answer any questions I had. I would also like to thank Ismaail Ghaaowd for helping me develop the pulley system that was used in the study and helping me fix problems that arose with the pullout device. I would finally like to thank Candice Hanna for her help with the construction of the specimens.

Finally, I would like to dedicate this thesis to my parents for their love and support as well as their continuous encouragement throughout my years of study and throughout this entire thesis process. I would not be where I am today in this journey without them and the values they have bestowed upon me. A sincere thank you for everything they have done for me.

Financial support for this research was provided by National Science Foundation (NSF) Civil, Mechanical and Manufacturing Innovation (CMMI) Grants 1054190 and 1230237, and is gratefully acknowledged.

ABSTRACT OF THE THESIS

Temperature Effects on Pullout of Woven Geotextiles

from Unsaturated Silt

by

Bernardo Ambriz

Master of Science in Structural Engineering

University of California, San Diego 2018

Professor John S. McCartney, Chair

This study investigates the effect of temperature on the interaction mechanisms between reinforcing geotextiles confined in unsaturated, compacted silt. The results and analysis from this study are relevant to the evaluation of the effects of incorporating geothermal heat exchangers into mechanically-stabilized earth (MSE) retaining walls constructed with poorly draining backfill. A thermo-mechanical geosynthetic pullout device was used in this study that incorporates standard

components for geosynthetic pullout or creep testing including a rigid soil box with an integrated vertical loading system, a roller grip to apply pullout forces uniformly to the geotextiles, a pulley system for load-controlled creep testing, a servo-motor for displacement-controlled monotonic pullout testing, and instrumentation for monitoring vertical settlement, pullout force, and pullout displacement measurements. Further, the pullout device incorporates heating elements at the top and the bottom of the soil box to apply constant temperature boundary conditions to the soil layer as well as dielectric sensors embedded at different depths in the soil layer to monitor the soil temperature and volumetric water content. Two sets of pullout tests were performed on geotextiles within compacted silt layers having initial degrees of saturation of 0.44. The first involves monotonic pullout of a woven polypropylene (PP) geotextile after reaching steady-state conditions under different boundary temperatures without a seating load, and the second involving monotonic pullout of a woven polyethylene-terephthalate (PET) geotextile after reaching steady-state conditions under different boundary temperatures while under a constant seating pullout load. The second testing series permits evaluation of possible thermally-induced creep displacements. The boundary temperatures investigated in this study are typical of geothermal heat exchange systems and range from 20 to 50 °C. These temperatures are lower than the glass transition temperature of the PET geotextile but greater than that of the PP geotextile.

The results from the two testing series indicate that the ultimate pullout resistance of the geotextiles heated with and without a seating load decreased with increasing temperature. Although heating led to drying of the silt layer throughout most of its height, as expected, water was observed to accumulate at the soil-geotextile interfaces leading to an increase in degree of saturation at this location. An effective stress analysis considering thermal softening mechanisms in soils indicates that the increase in degree of saturation at the soil-geotextile interface was the

primary cause of the decrease in pullout resistance. The rate of decrease in ultimate pullout resistance with temperature was similar for both geotextiles tested, indicating that application of temperatures to the polypropylene geotextile greater than its glass transition temperature do not have a major effect on its nonisothermal response.

Chapter 1

Introduction

1.1 Motivation

Mechanically-Stabilized Earth (MSE) walls are cost-effective soil retaining structures that can tolerate relatively large settlements or facing displacements without reaching failure (Berg *et al.* 2009). The underlying concept of MSE walls is the placement of tensile reinforcing elements (i.e., geogrids, geotextiles, metallic strips, etc.) during compaction of backfill soil to form a self-supporting soil-geosynthetic composite material. MSE walls typically have a vertical concrete block facing that is intended for aesthetics and not meant to provide structural support. The internal stability and deformation response of MSE walls depends on the tensile strength and creep characteristics of the reinforcements, the shear strength of the backfill soil, and soil-geosynthetic interaction. The presence of water may also play an important role in MSE wall behavior, as the additional weight water will increase the driving force for failure and reduce the effective stress state within unsaturated backfill soil. Water has a more significant effect on backfill soils with low hydraulic conductivity, referred to as poorly draining backfill soils (Zornberg and Mitchell 1994, Zornberg *et al.* 1995). Infiltration and evaporation due to environmental interaction along with changes in the groundwater table can lead to changes in the pore water pressure and effective stress in the soil, which may lead to deformations for poorly draining backfill soils.

To minimize issues arising from these changes in the backfill effective stress state, MSE wall design codes specify the use of free-draining backfill soils having a low fines content within the reinforced zone (e.g., Berg *et al.* 2009). However, in some cases, free-draining soils are not readily available or may be too expensive for a project, so an alternative is to use non-ideal, poorly-draining backfill soils (i.e., silts and clays) that may be available on the site. A few studies have found that under optimal conditions these poorly draining backfill soils can have acceptable performance, especially when the backfill soil remains unsaturated (Zornberg and Mitchell 1994, Zornberg *et al.* 1995). However, infiltration of water and slow drainage rates lead to reductions in the effective stress in the unsaturated backfill, which may lead to reductions in the shear strength and stiffness of the backfill (Lu *et al.* 2010; Khosravi and McCartney 2012). One approach to reduce the negative effects of using poorly-draining backfill soils in MSE walls is to incorporate strategies to ensure that the backfill soils remain unsaturated.

One possible strategy that has been proposed is to incorporate geothermal heat exchangers into MSE walls to induce drying of backfill soils by thermally-induced water flow. Different configurations of earthen structures with geothermal heat exchangers have been proposed, including thermally-active MSE walls (Stewart and McCartney 2013; Stewart *et al.* 2014a) and thermally-active embankments (Coccia and McCartney 2013). These systems can be used to dissipate excess heat from power plants or buildings, making cooling systems become more environmentally friendly. Integrating MSE walls into the energy infrastructure may potentially make their construction be more economical by offsetting costs associated with energy infrastructure cooling requirements. As MSE walls already incorporate several subsurface technologies including geosynthetics and drainage components (i.e., blanket or chimney drains), inclusion of additional plumbing for geothermal heat exchangers is not expected to create a

significant increase in their cost or complexity. A conventional MSE wall showing the typical configuration of geosynthetic reinforcements in the backfill soil is shown in Figure 1.1(a), while a thermally-active MSE wall with different configurations of geothermal heat exchangers is shown in Figure 1.1(b). Specifically, one configuration involves placing the geothermal heat exchangers and geosynthetic reinforcements in alternating lifts (in which case water flow will be from the geothermal heat exchangers toward the geosynthetic reinforcements). The second alternative configuration involves placing the geothermal heat exchangers and geosynthetics in the same lift (in which the water flow will be away from the geosynthetic reinforcements but the temperatures will be higher at the locations of the reinforcements). The boundary conditions of the experiments performed in this study are consistent with the first configuration.

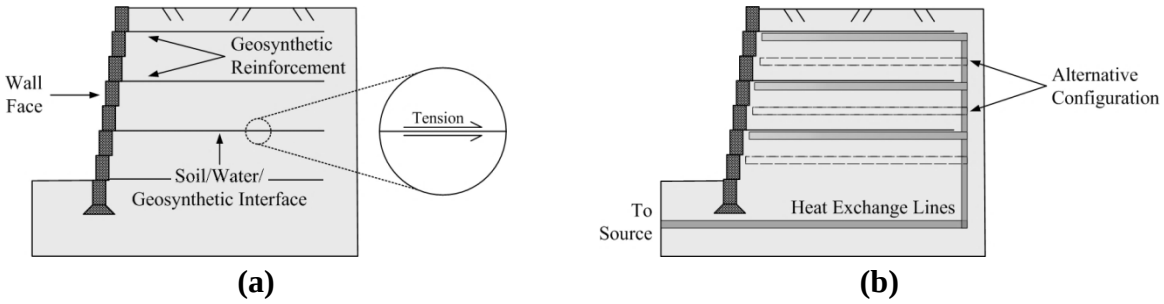

Figure 1.1 Simplified elevation of typical configuration of an MSE Wall: (a) Conventional MSE wall; (b) Thermally-active MSE wall showing geosynthetic heat exchangers in the reinforced backfill soil

One challenge that arises when incorporating geothermal heat exchangers into MSE walls is that the injection of heat may lead to a change in the behavior of the soil and geosynthetic reinforcements, which must be understood before this technology is implemented in practice. On the positive side, thermally-induced flow of water away from the geothermal heat exchangers is expected to occur in unsaturated soils (i.e., Philip and De Vries 1957). This will lead to a lower degree of saturation, increased suction, and increased effective stress in the backfill soil at the locations of the heat exchangers (Coccia and McCartney 2013). If geotextiles are used as the

reinforcing geosynthetic in the MSE wall, they may also act as lateral vapor drains, helping to expel water from the backfill (Stewart *et al.* 2014b). Despite the positive effects of heating, it is well known that heating of geosynthetics in unconfined conditions (Zornberg *et al.* 2004; Bueno *et al*. 2005) and confined conditions (Karademir 2011) leads to accelerated creep. This may lead to additional lateral displacements in thermally-active MSE walls, which can be referred to as thermal softening (Stewart *et al.* 2014a). The interaction between suction-induced hardening of the unsaturated soil and thermal softening of the geosynthetic reinforcements must be carefully quantified for the soil and geosynthetics used in a thermally active MSE wall. Specifically, it is important to consider the behavior of geosynthetics confined in unsaturated backfill soil under nonisothermal conditions when determining whether the positive influence of a decreased degree of saturation in the backfill soil offsets the negative aspects of thermal softening.

1.2 Objectives

The primary objectives of this study are to:

1. characterize the interaction between woven reinforcing geotextiles and compacted poorly-draining backfill soil during application of different temperature boundary conditions to the soil layer, including both the load-displacement pullout response and the ultimate pullout capacity;
2. apply measurements of the spatial and temporal changes in temperature, volumetric water content (and indirectly the matric suction), and volume change in the soil after reaching steady-state conditions under different temperature boundary conditions in an effective stress analysis to interpret the nonisothermal pullout results.

1.3 Approach

The approach used in this study to characterize the effects of thermal softening on the behavior of reinforcing geosynthetics confined in compacted soil, is presented in a series of test results performed using a thermo-mechanical pullout device. The device was originally developed by Carpenter *et al.* (2015), but was updated in this study to perform creep tests under a constant mechanical load and pullout tests at a constant displacement rate. The pullout device incorporates standard components including a rigid soil box with an integrated vertical loading system, a roller grip to apply pullout forces uniformly to the geotextiles, a pulley system for load-controlled creep testing, a servo-motor for displacement controlled monotonic pullout testing, and instrumentation for monitoring vertical settlement, pullout force, and pullout displacement measurements. The box also incorporates heating elements at the top and bottom of the box, along with an array of dielectric sensors embedded in the soil for measurement of temperature and volumetric water content. The testing program is configured to understand the baseline pullout behavior of geotextiles under room-temperature conditions as well as the effects of transient heat transfer and water flow through the unsaturated backfill soil on the pullout creep and monotonic pullout of a woven geotextile. Results obtained from tests performed with this device will not only provide new insight into geosynthetic behavior but can be used to validate and enhance simplified analytical models to predict the temperature-induced facing deflections of thermally active MSE walls, such as the analytical model developed by Stewart *et al*. (2014a).

1.4 Organization

The remainder of the thesis is organized in the following manner:

- Chapter 2 presents a literature review on concepts and previous works pertaining to effective stress in unsaturated soils and its role in shear strength, effects of temperature on the hydraulic and thermo-mechanical response of unsaturated soils, soil-geosynthetic interaction characterization using pullout testing, thermal effects on geosynthetics, and soil-geosynthetic interactions in pullout tests. This chapter also includes a review of heat transfer and water flow processes in thermally active MSE walls, and models for the deflection of thermally-induced MSE walls.
- Chapter 3 presents a detailed description of the materials and methods used in this study. This includes details of the pullout box, properties of the soil and geosynthetics used in this study, instrumentation, specimen construction, and different test configurations that were investigated in the pullout tests.
- Chapter 4 presents results from the two testing series on the nonisothermal pullout behavior of geotextiles with and without a seating pullout load during heating (pullout load-displacement curves and ultimate pullout resistance), along with observations of the thermo-hydro-mechanical soil behavior due to the thermal loading.
- Chapter 5 presents an effective-stress analysis of the ultimate pullout capacity as a function of temperature and degree of saturation.
- Chapter 6 presents conclusions drawn on the experimental testing program and analysis, along with recommendations for future research.

Chapter 2

Literature Review

2.1 Effective Stress in Unsaturated Soils

Before evaluating the pullout response of geotextiles for unsaturated soils, it is important to understand and quantify the effective stress state. The effective stress is the key parameter in geotechnical engineering that governs the stress-strain deformation response and shear strength of soils. Similar to saturated soils, unsaturated soils experience changes in volume, shear strength, and stiffness in response to changes in effective stress (Khalili *et al*. 2004; Lu *et al*. 2010; Khosravi and McCartney 2012). However, because unsaturated soils are three-phase systems, the definition of effective stress is different as it must account for the effects of the pore air and pore water pressures in soil, as well as the relative quantity of air and water in the soil. The difference in pore air and pore water pressures is referred to as the capillary pressure or matric suction. The mechanical deformation and hydraulic changes in unsaturated soils take place simultaneously under external loads, with the degree of saturation playing a key role in the soil behavior (Sun *et al.* 2010). To account for the role of degree of saturation in volumetric response, the effective stress approach of Bishop (1959) was adopted in this study, where the mean effective stress σ' in unsaturated soils is expressed as follows:

$$\sigma' = \sigma_{net} + \chi\psi \tag{2.1}$$

where σ_{net} is the net normal stress equal to the total normal stress in excess of the pore air pressure (i.e., σ-u_a), ψ is the matric suction (u_a-u_w), and χ is the effective stress parameter. Equation 2.1 can

be applied to normal stresses in any direction or to the mean stress. The value of χ can be defined using several different approaches, but in this study it is assumed to be equal to the effective saturation S_e following the approach of Bolzon and Schrefler (1998) and Lu *et al*. (2010). The effective saturation is defined as follows:

$$S_e = \frac{S_r - S_{r,res}}{1 - S_{r,res}} \tag{2.2}$$

where S_r is the degree of saturation and $S_{r,res}$ is the residual saturation for a given soil (assumed to be a constant value). The value of S_e varies from 1 to 0 as the soil transitions from saturated conditions to residual saturated conditions, respectively. An implication of choosing $\chi = S_e$ is that the soil-water retention curve (SWRC) can be directly integrated into the definition of the mean effective stress (Lu *et al.* 2010). The SWRC is a fundamental relationship in unsaturated soils that relates the amount of water in the soil, which can be quantified by the effective saturation, and the energy state in the pore water, which can be quantified by the suction. A common SWRC model is that of van Genuchten (1980), given as follows:

$$S_e = \left\{\frac{1}{1 + [\alpha(u_a - u_w)]^n}\right\}^{1-\frac{1}{n}} \tag{2.3}$$

where α and n are fitting parameters that depend on the soil type.

The product of the effective stress parameter and suction can be referred to as the suction stress σ^s (Lu and Likos 2006). As the form of Equation 2.1 indicates that the suction stress will vary with suction and effective saturation, the relationship between the suction stress with either parameter is referred to as the suction-stress characteristic curve (SSCC). Suction stress is important in interpreting the shear strength of soils, and can be used to relate the peak shear strength or the critical state shear strength to the effective stress (Lu *et al.* 2010; Khosravi *et al.*

2012). This study is focused on the peak shear strength between soil and a geosynthetic reinforcement during pullout. In this case, for a horizontal interface between soil and another material, the peak shear strength can also be defined as follows:

$$\tau_f = \sigma' tan\phi' \tag{2.4}$$

where ϕ' is the friction angle and σ' is defined using Equation 2.1.

2.2 Thermal Effects on Unsaturated Soils

The first way that temperature can affect the behavior of unsaturated soils is that the shape of the SWRC may change due to the effects of temperature on water-air surface tension and water-solid contact angle. These effects were considered by Grant and Salehzadeh (1996), who modified the van Genuchten (1980) SWRC to account for temperature, as follows:

$$S_e = \left(\frac{1}{\left(\alpha_{GS} \psi_{,T=T_r} \left(\frac{\beta_0 + T_r}{\beta_0 + T_f} \right) \right)^{\lambda_{GS}} + 1} \right)^{\frac{\lambda_{GS}-1}{\lambda_{GS}}} \tag{2.5}$$

where T_r is a reference temperature before heating (Kelvin), T_f is the final temperature after heating (Kelvin), α (kPa^{-1}) and λ are the fitting parameters for the van Genuchten SWRC, and β_o is an empirical parameter. A value of β_o equal to 400K was observed to provide a reasonable value for silts under drained conditions (She and Sleep 1998). This equation for the nonisothermal SWRC can be multiplied by the suction to define the nonisothermal SSCC using the assumption of Lu *et al.* (2010), as follows:

$$\sigma^s = \psi * \left(\frac{1}{\left(\alpha_{GS} \psi_{T=T_r} \left(\frac{\beta_0 + T_r}{\beta_0 + T_f} \right) \right)^{\lambda_{GS}} + 1} \right)^{\frac{\lambda_{GS}-1}{\lambda_{GS}}} \quad (2.6)$$

The next way that temperature may affect the behavior of unsaturated soils is through thermally-induced water flow, which may lead to changes in suction and degree of saturation within the space around a heat source/sink in the unsaturated soil layer. For example, Philip and De Vries (1957) observed that when unsaturated soils are heated, water will move from regions of high temperature to low temperature in liquid form due to the impacts of temperature on water density, water-air surface tension, and water vapor pressure. In short, water vapor will evaporate from the heating front, diffuse away from the heating front due to the vapor pressure gradient, and condense in a cooler region of the soil layer. Water and water vapor will also rise upward due to buoyancy as the density of these materials decrease with temperature. The rate of diffusion of water vapor through unsaturated soils is also greater than the diffusion of water vapor through air due to the concept of liquid islands, introduced by Philip and De Vries (1957), which assumes that water will evaporate and condense on water islands retained at the particle contacts to increase the area available for water vapor diffusion through the unsaturated soil. The main factors that affect the zone of influence of liquid and vapor movement are initial saturation, hydraulic conductivity, thermal conductivity and porosity (Thomas *et al.* 1996). Coccia and McCartney (2013) performed a numerical analysis using VADOSE/W to understand the influence of initial saturation on a layer of unsaturated silt with a horizontal heat exchanger, and found that the lower the initial degree of saturation, the more thermally induced water flow occurred. This can be observed in the simulation results shown in Figure 2.1(b). Coccia and McCartney (2013) also observed that although changes in temperature may occur across the entire soil layer at steady-state conditions, the zones of drying

(decrease in degree of saturation) occurred in a smaller region up to approximately 0.3 m away from the heat exchanger. It was concluded that the decrease in degree of saturation near the heat exchanger will ultimately lead to a considerable influence on the effective stress at this location, through the previously mentioned correlation between the effective saturation and suction stress.

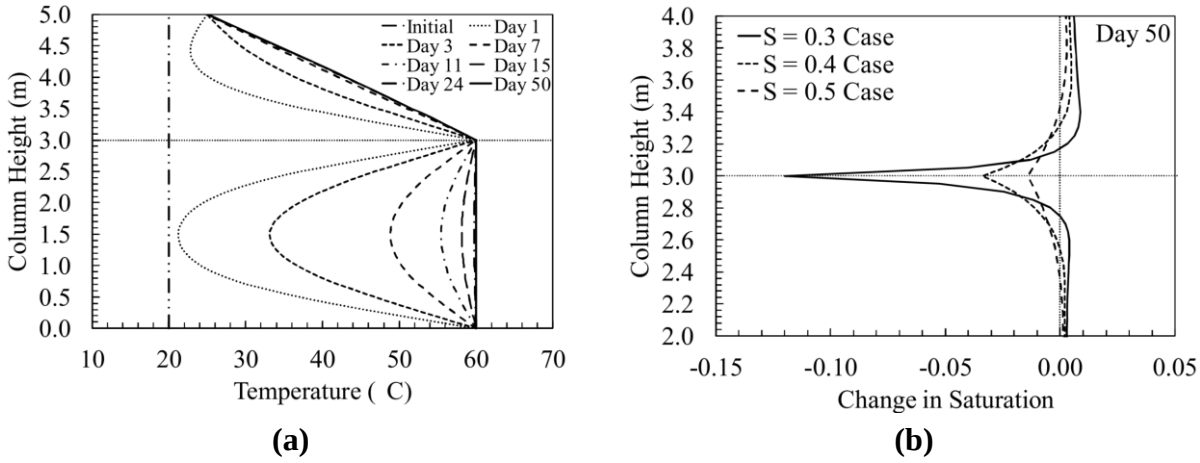

Figure 2.1 Numerical model of earthen embankment with horizontal heat exchanger: (a) Temperature profiles; (b) Change in degree of saturation within 2 m of central heat exchanger (from Coccia and McCartney 2013)

Temperature can also affect unsaturated soils by inducing changes in volume. It has been observed that heating of an unsaturated soil element under drained conditions can cause either expansive or contractive behavior depending on the stress history of the soil (Hueckel *et al.* 1990). Alsherif and McCartney (2016) found that the impacts of stress history for unsaturated soils are similar to those of saturated soils when the current stress state and the preconsolidation stress are quantified in terms of effective stress using Equation 2.1 and verified this by comparing data on Bonny silt reported by Vega and McCartney (2015) and Alsherif and McCartney (2015). Uchaipichat and Khalili (2009) performed constant water content heating tests on compacted silts and measured the decrease in matric suction for different temperatures. They observed that overconsolidated unsaturated soil specimens exhibit elastic thermal expansion during heating and cooling, such as those in Figure 2.2(a), while normally consolidated to lightly overconsolidated

unsaturated soils, such as those in Figure 2.2(b), exhibit plastic contraction during heating. The underlying mechanisms causing the thermal contraction of normally consolidated unsaturated soils are complex, and still not fully understood (Coccia and McCartney 2016a; 2016b).

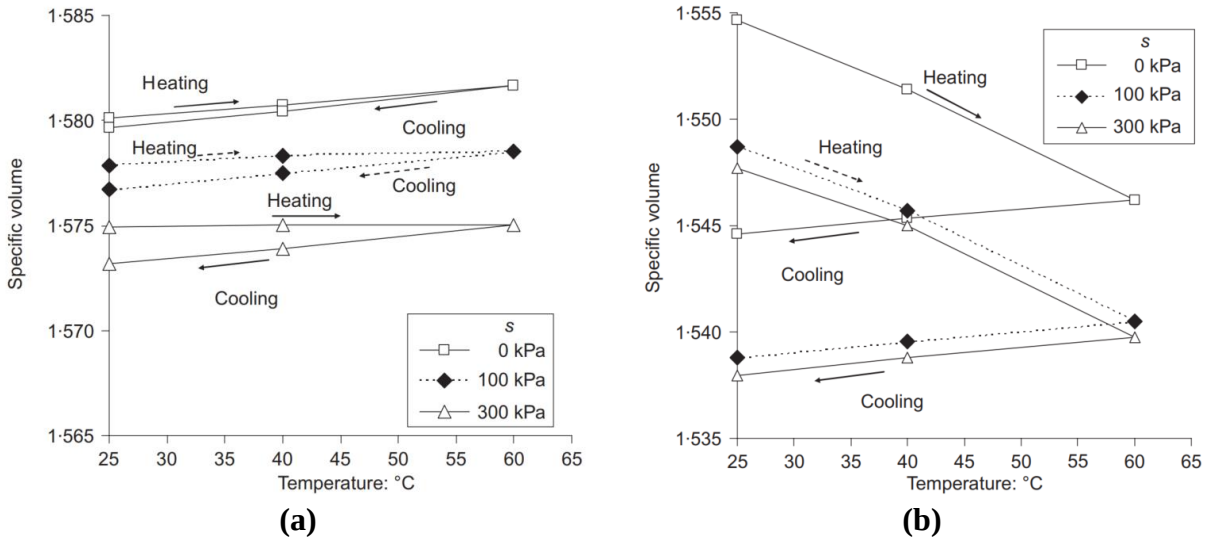

Figure 2.2 Specific volume against temperature at different matric suctions (from Uchaipichat and Khalili 2009): (a) Tests under a net stress of 50kPa (higher OCR); (b) Tests under a net stress of 200kPa (lower OCR)

Temperature typically does not have a significant impact on the material properties of most unsaturated soils. For example, temperature has been observed to have a negligible effect on the compression indices of the saturated and unsaturated soils (Campanella and Mitchell 1968; Saix *et al.* 2000; Uchaipichat and Khalili 2009) and soil friction angle or critical state line (Cekerevac and Laloui 2004; Uchaipichat and Khalili 2009). Although temperature does not directly impact the mechanical properties, it does influence the shear strength of soils through thermal changes in void ratio, changes in suction stresses, and a decrease in preconsolidation stress (Uchaipichat and Khalili 2009). The decrease in preconsolidation stress with temperature will lead to a reduction in stiffness and a softer stress strain curve of the soil.

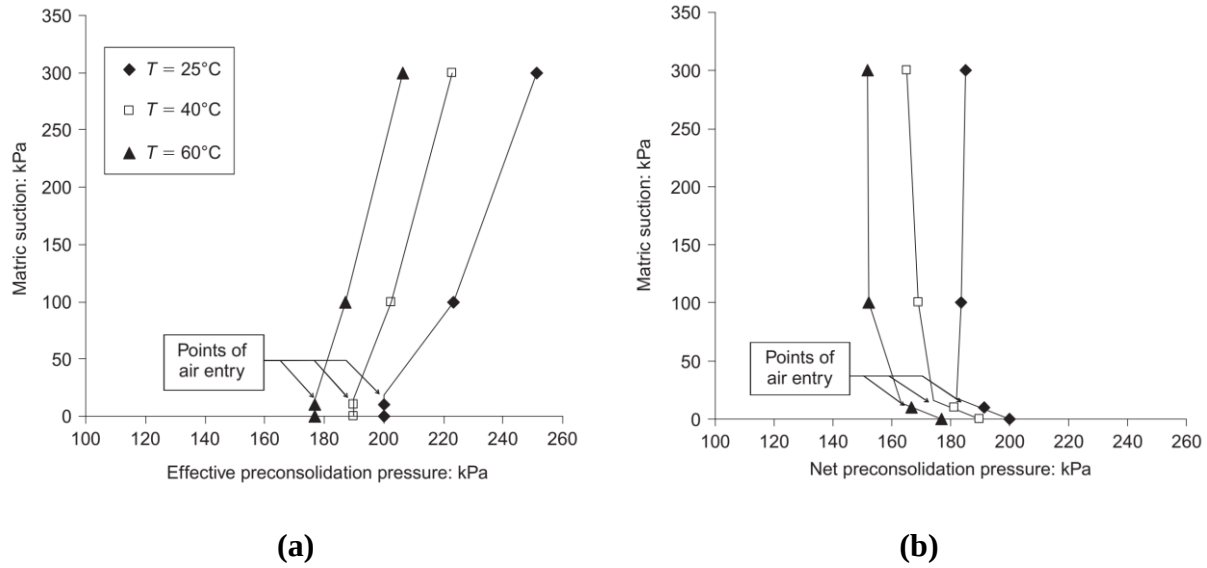

Figure 2.3 Loading collapse (LC) curves at different temperatures in terms of: (a) Effective Preconsolidation Stress; (b) Net Preconsolidation Stress (from Uchaipichat and Khalili 2009)

The stress-strain curves from the temperature- and suction-controlled triaxial compression shear tests from Uchaipichat and Khalili (2009) are shown in Figure 2.4, for different confining stresses. In their study, they interpreted stress-strain curves in terms of critical state soil mechanics and concluded that temperature has a negligible effect on the shear strength at critical state conditions (i.e., at large strains). However, their results indicate that temperature may have a major effect on the peak shear strength, with a softening effect leading to a decrease in peak shear strength with increasing temperature. Evaluation of the stress-strain curves also indicates that an increase in suction leads to a greater increase in peak shear strength than the decrease in peak shear strength due to heating. The trends in peak shear strengths with temperature for silt having different suction values are shown in Figure 2.5. These trends will be used in Chapter 5 when analyzing different effects of temperature and drying on the pullout resistance of geotextiles embedded in unsaturated compacted silt.

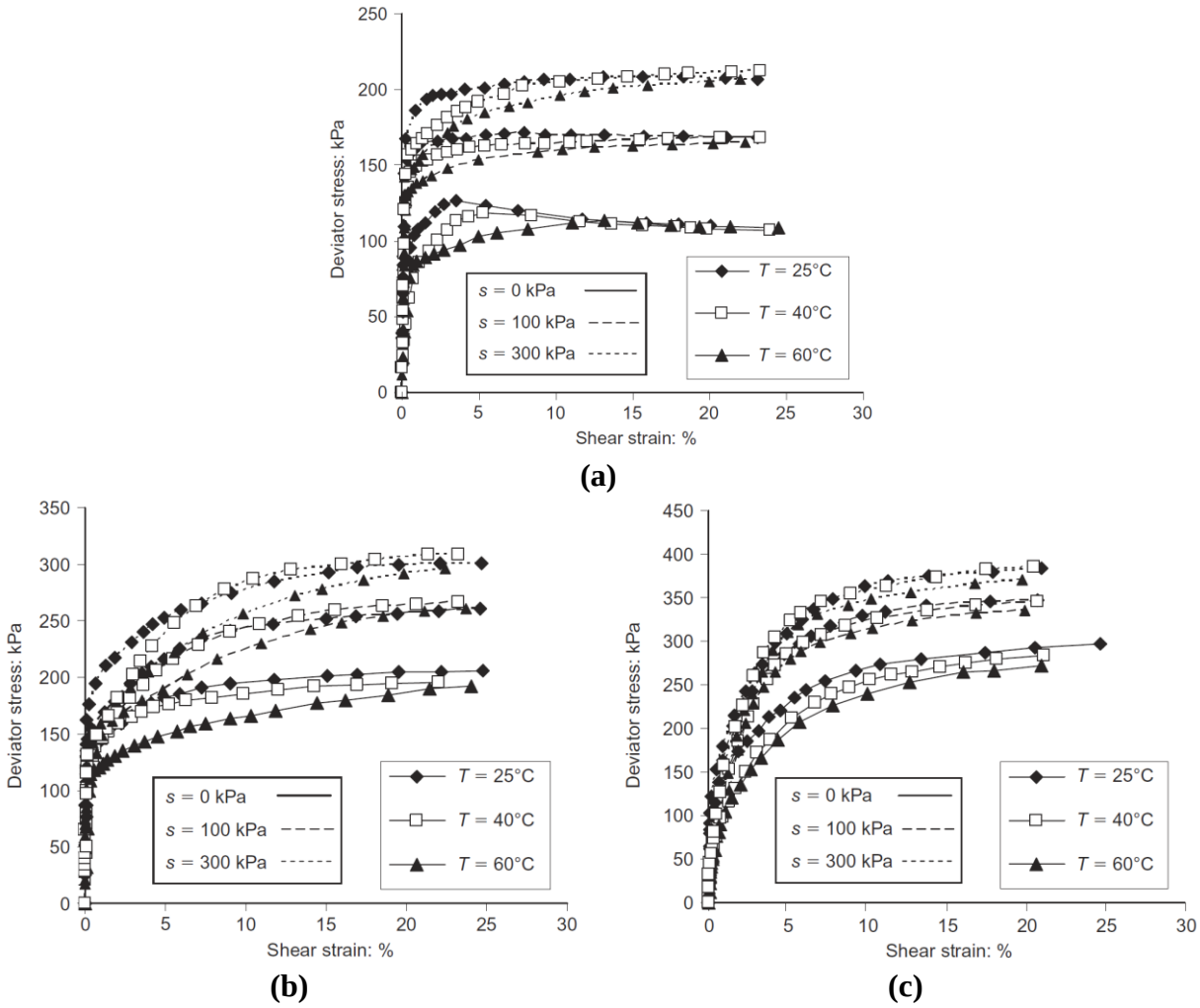

Figure 2.4 Temperature- and suction-controlled conventional compression shear tests: (a) initial mean effective stress of 50 kPa; (b) initial mean effective stress of 100 kPa; (c) initial mean effective stress of 300 kPa (from Uchaipichat and Khalili 2009)

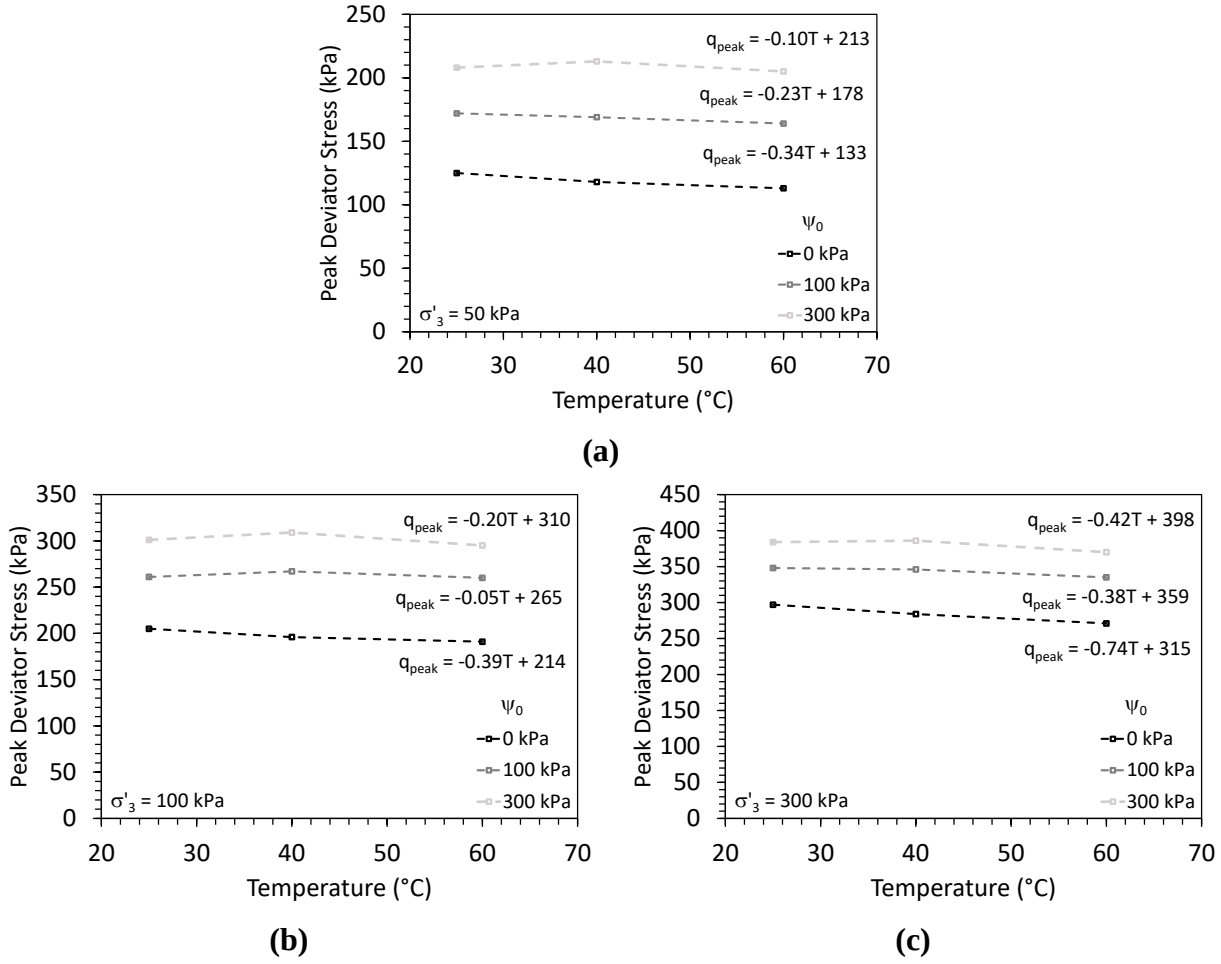

Figure 2.5 Peak shear strengths from temperature- and suction-controlled conventional shear tests: (a) initial mean effective stress of 50 kPa; (b) initial mean effective stress of 100 kPa; (c) initial mean effective stress of 300 kPa

2.3 Geosynthetic Tensile Strength and Confining Stress Effects

The stress-strain behavior of a geosynthetic is often represented in terms of a force-displacement (P-d) curve as they are planar in structure. The tensile force P is defined in terms of force per unit width. Their tensile stiffness is given as the tangent slope of the P-d curve in the elastic region, whereas their ultimate tensile strength is defined as the maximum load before rupture. As geosynthetics behave in a relatively elastic manner, except near rupture, it is important to determine the creep potential as large displacements may lead to creep rupture. Another factor that is important in predicting the in-situ stress-strain response is the confining pressure on a

geosynthetic. McGown *et al.* (1982) observed that the tensile strength of geotextiles under confined and unconfined conditions indicated that the stiffness of the geotextile increased with an increase in confining pressure. The results in Figure 2.6 show how a geotextile behaves under different confining conditions. The results indicate that when the geotextile is confined under a constant confining stress there is far less creep/rupture potential than when the same specimen is unconfined. A hypothesis that has been proposed by Bueno *et al.* (2005) is that confining pressure prevents necking (or reduction in transverse strains) of the geosynthetic leading to larger stiffness. However, it is very difficult to perform confined tensile shear strength tests to fully confirm this assumption.

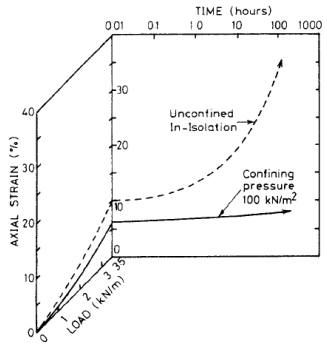

Figure 2.6 Load-strain relationship for geotextile under confined and unconfined conditions (from McGown *et al.* 1982)

2.4 Thermal Effects on Geosynthetic Stiffness

The tensile stiffness of a geosynthetic with respect to a change in temperature is based on the polymer used and the corresponding glass transition temperature (T_g). This property defines how the plastic will behave with a change in temperature (i.e., stiff or brittle). If the glass transition temperature is not exceeded then there will be no change in the material stiffness, yet there will still be creep or creep potential change. That is, regardless of the glass transition temperature, the

larger the temperature increase the higher the creep. This was observed in this study during the thermal loading of the pullout tests.

The strain relationship of a geotextile under thermal applications is shown in Figure 2.7. Stewart *et al.* (2013) hypothesized that an increase in temperature of a geosynthetic will lead to greater creep displacements under the same tensile force where the ambient temperature creep would be the minimum, which can be observed in Figure 2.7(a). This can also be represented by combining the elastic and creep displacements at steady-state conditions to define the modified secant stiffness under a given temperature (J_{creep}), which is defined as the change in displacement as a function of the tensile force, as observed in Figure 2.7(b).

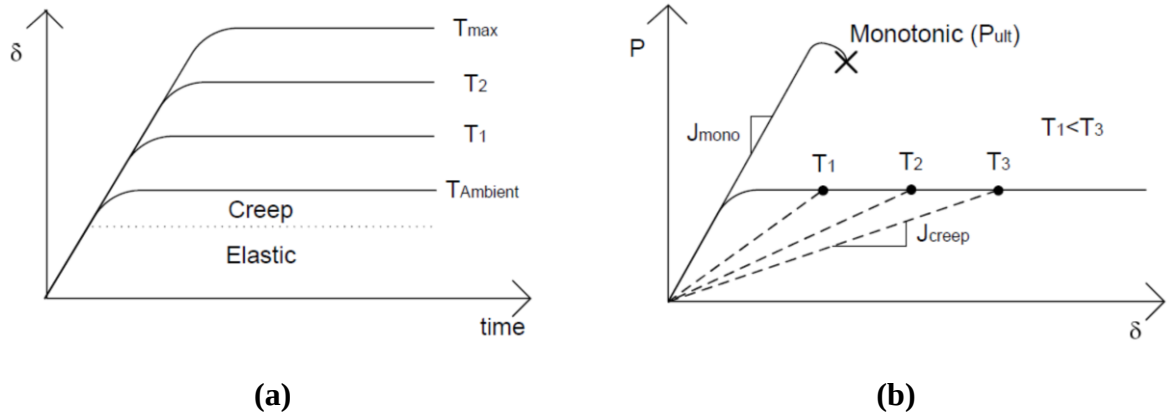

Figure 2.7 Stress-strain behavior of geosynthetics in thermally active conditions: (a) deflection as a function of P_{ult} applied; (b) deflection as a function of time (from Stewart *et al.* 2013)

2.5 Soil-Geosynthetic Interaction in Pullout Tests

Soil-geosynthetic interaction mechanisms are typically assessed using geosynthetic pullout tests. These tests involve application of tensile stresses to a reinforcing geosynthetic combined in a layer of compacted soil to characterize the pullout resistance. The pullout resistance from such a

test is also relevant in assessing the stability of MSE walls, as it is useful in quantifying the necessary length of geosynthetic reinforcements to provide sufficient anchorage of a failure wedge.

The minimum dimensions of a pullout box for geosynthetic pullout are defined in ASTM D6706. These dimensions were defined to account for boundary effects that can affect the pullout tests, which include side wall, front and back wall, and top and bottom boundary effects. An example of a pullout box that meets the requirements of ASTM D6706 is shown in Figure 2.8.

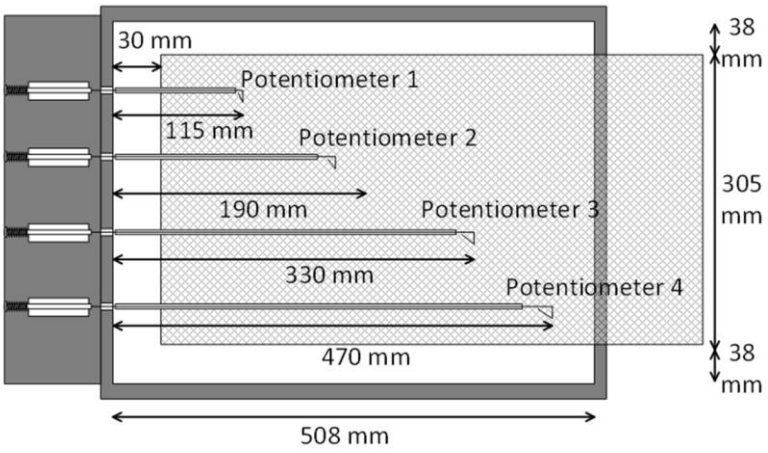

Figure 2.8 Plan view of pullout box meeting the requirements of ASTM D6706 (from Carpenter *et al.* 2015)

Side wall boundary effects occur when frictional resistance is mobilized along the side walls of the pullout box. Farrag *et al.* (1993) performed a study on the pullout resistance of geogrids that included evaluating the side wall effects as a function of the distance from the edge of the geosynthetic to the sidewall. The results from that study are presented in Figure 2.9. It is apparent that the effects of mobilized wall friction on the pullout resistance increases with confining stress. This is primarily due to larger soil deformations with an increase in confining pressure leading to additional frictional resistance. Side wall boundary effects can also be mitigated using different materials that can reduce the friction between the soil and the walls (i.e.,

grease, foam sheets, plastic sheets). In this study, plastic sheets were placed on the side walls to reduce the side wall friction to more accurately represent the pullout resistance.

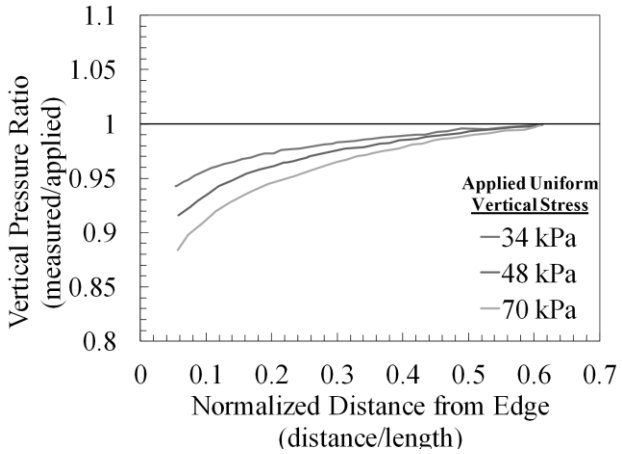

Figure 2.9 Vertical pressure ratio (measured/applied stress) as a function of distance from the side wall (from Farrag *et al.* 1993)

During pullout of a geotextile friction with the soil will lead to development of passive pressure between the soil and the front wall of the pullout box. This typically results in an increase in the measured pullout resistance. This effect is mitigated by installing bearing sleeves attached to the top and bottom opening to reduce front wall boundary effect. Chang *et al.* (2000) performed an investigation on the effects of the sleeve lengths and found that after including bearing sleeves with a length of 15 mm there were minimal effects to the measured pullout resistance, as shown in Figure 2.10. The edge effects of the back wall were not considered in this study as the interface between the back wall and the backfill soil is assumed to have negligible tensile strength.

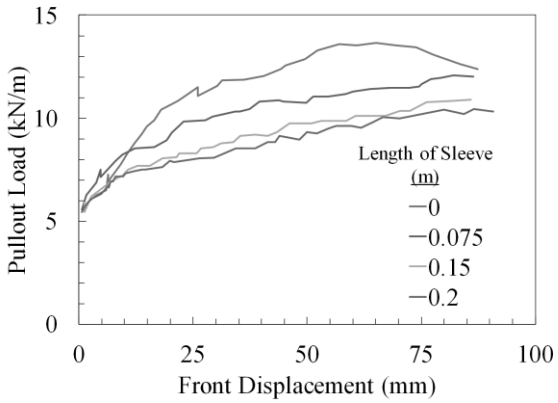

Figure 2.10 Displacement-controlled pullout load with varying length of bearing sleeve in pullout box opening (from Chang *et al.* 2000)

The top and bottom plates of a pullout box have similar effects as the side walls. This is due to the mobilization of the soil along the interface caused by friction. Brand and Duffy (1987) performed a study on a geogrid embedded in clay to observe the effects of the height of soil cover on the pullout response. It was found that after a height of soil cover of about 65 mm, the soil cover had little effect on the pullout force of the geogrid as shown in Figure 2.11.

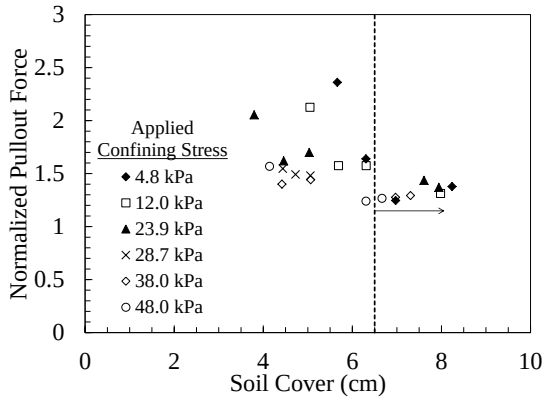

Figure 2.11 Normalized pullout force as a function of soil cover depth (Brand and Duffy 1987)

Chapter 3

Materials and Methods

3.1 Testing Apparatus

The testing apparatus used in this study was adapted from the thermo-hydro-mechanical box developed by Carpenter *et al.* (2015) to measure the pullout resistance of geosynthetics from unsaturated soils under elevated temperatures. Schematics of the thermo-hydro-mechanical pullout box are shown in Figures 3.1(a) and 3.1(b), while a photograph of the apparatus is shown in Figure 3.1(c). The main difference between the original device developed by Carpenter *et al.* (2015) and this study is the mode by which the pullout load is applied, which was modified to perform pullout tests on geosynthetic reinforcements in both load-control conditions (i.e., to evaluate creep under constant load) as well as in displacement-control conditions (i.e., to evaluate monotonic pullout to failure). The pullout load is applied to the geosynthetic using a combination of a dead-weight system, which facilitates evaluating creep under constant load, and a linear actuator, which facilitates the monotonic geosynthetic pullout. A roller grip on a sliding frame is used to grip the geosynthetic to apply uniform horizontal pullout loads. A Bellofram pneumatic piston is used to apply vertical loads to the rigid plate on the top of the soil specimen. Although application of vertical stresses using a rigid plate may lead to stress concentration issues, the top place of the pullout device contains eating elements, which will be described below.

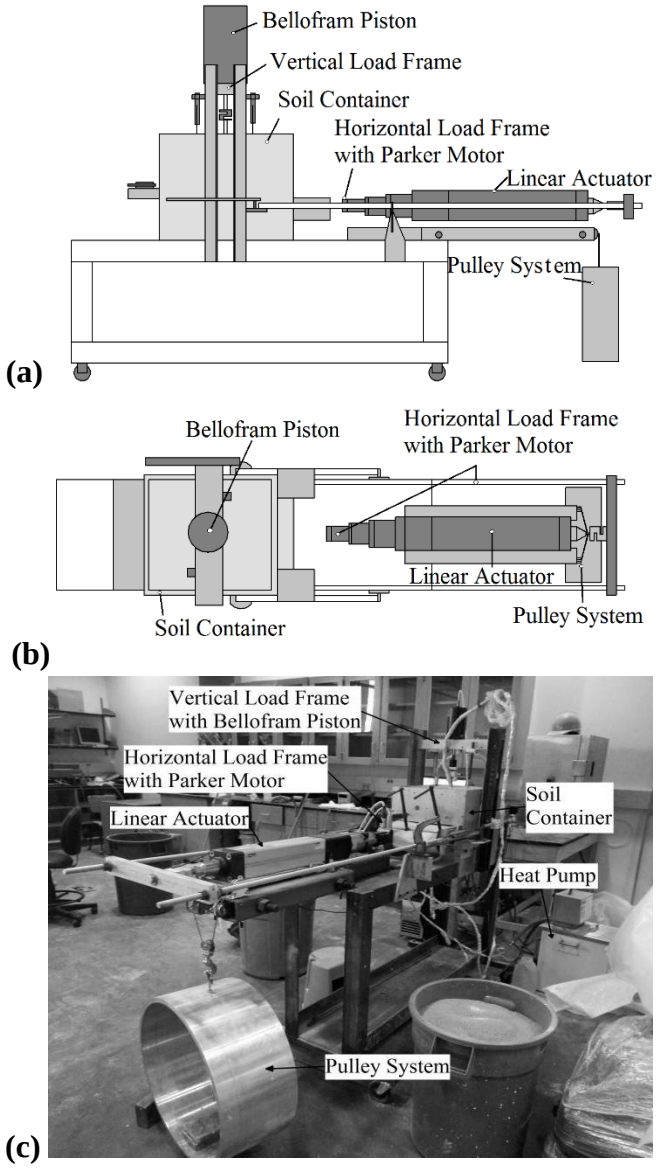

Figure 3.1 Pullout device: (a) Elevation view schematic; (b) Plan view schematic; (c) Picture showing the different components

Schematics showing the internal dimensions of the soil container are shown in Figure 3.2, along with the locations of the instrumentation embedded in the soil mass. Dielectric sensors (model 5TM from Decagon Devices) were embedded at different depths and were used to monitor changes in both temperature and volumetric water content in the soil layers during heating. Since the apparatus is not designed to control the suction within the soil layers during testing, the dielectric sensors are used to infer changes in degree of saturation during the heating process, and

the suction can be inferred using the SWRC. A long-stroke (150mm) linearly variable differential transformer (LDVT) was used to measure the face displacements of the grip. Two load cells were used to monitor the vertical and horizontal loads, and two vertical LDVTs were used to measure the settlement and possible tilt of the top cap. The bottom of the soil container contains a 12 mm-thick Delrin plate with an embedded copper heating coil. The top plate of the device also includes a 12 mm-thick Delrin plate with an embedded copper heating coil beneath an aluminum plate and was designed to allow vertical stresses to be applied via the Bellofram piston while still permitting temperatures to be applied to the upper boundary of the soil layer. Delrin was used to constrain the heating coils as it has a low thermal conductivity compared to that of the aluminum plates.

The temperature of the soil can be controlled by circulating water through the copper heating coils at both the top and the bottom of the soil layer. The heating coils do not extend across the entire top or bottom width of the loading plates but were placed in a spiral form across the center of the plate. This means that the soil within 75 mm of the front and back edges of the container are not directly heated. However, the interaction zone of the geosynthetic was expected to only be in the center portion of the soil box due to both the presence of the passive bearing sleeve at the face of the container shown in Figure 3.2(a) and the fact that the geosynthetic did not extend all the way to the back of the container. An advantage of this approach was that the geosynthetic loading system (i.e., roller grips and unconfined geosynthetic) were unheated and are not affected by the thermally-induced creep. A circulating heat pump (model F25-Me from Julabo, Inc) was used to control the temperature of the fluid circulating through the loading plates to reach the desired boundary temperature applied to the soil.

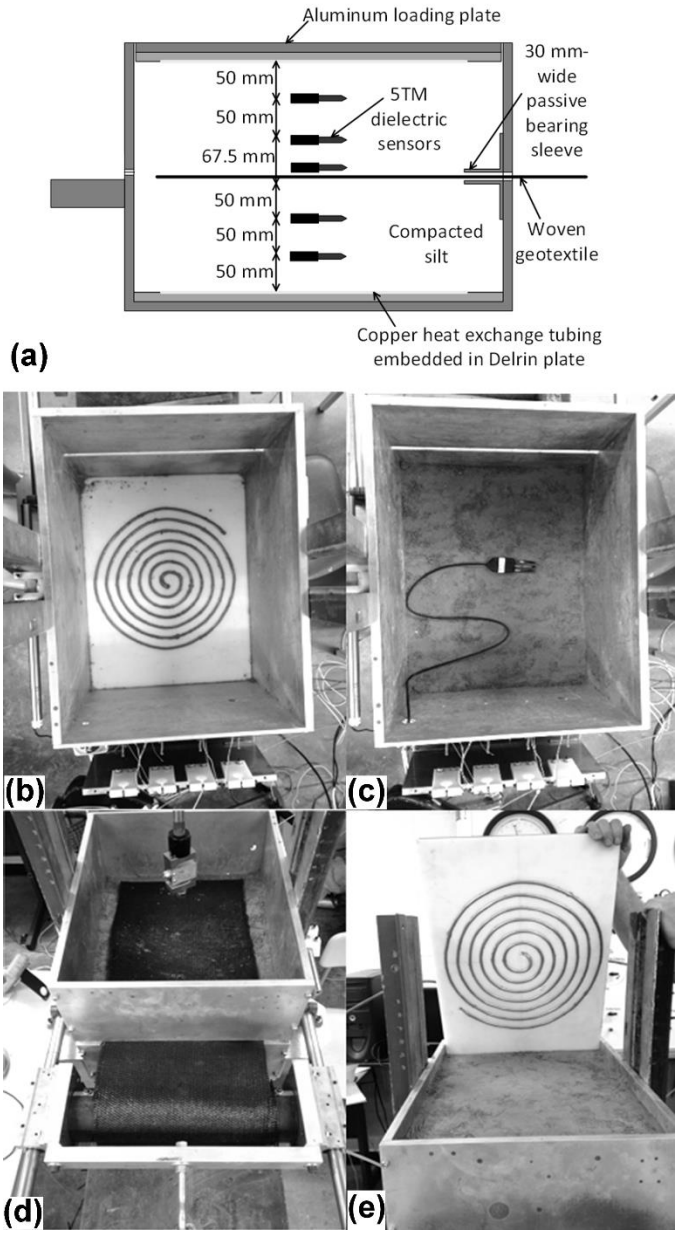

Figure 3.2 Inside of the pullout device: (a) Elevation view schematic; (b) Copper heat exchangers embedded into Delrin plates; (c) Dielectric sensor (temperature and volumetric water content) to be embedded in the soil; (d) Geosynthetic installation; (e) Upper loading plate with copper heat exchangers

3.2 Materials

Bonny silt was used in this study as it is an example of a poorly draining backfill that does not meet specifications for use in MSE walls (Berg *et al.* 2009). The soil has a fines content of 84%, and the liquid and plastic limits of the fines are 25 and 21, respectively, so the soil is classified

as ML (inorganic silt) according to the Unified Soil Classification Scheme (USCS). The silt also has a specific gravity of 2.6.

The silt was compacted into the pullout box using an impact hammer to a dry density of 1450 kg/m^3 at a gravimetric water content of 13.9%. This corresponds to an initial volumetric water content of 0.21 m^3/m^3, an initial porosity of 0.45, and an initial degree of saturation of 0.44. The initial thermal conductivity of the silt was 1.2 W/(m*K), which was measured using a KD2Pro thermal needle from Decagon Devices. The soil-water retention curve (SWRC) for Bonny silt at different temperatures was represented using the Grant and Salehzadeh (1996) model, as shown in Figure 3.3. It was observed that an increase in temperature leads to a slight downward shift in the SWRC so that the soil retains less water for the same suction. The suction stress characteristic curves predicted from these SWRCs using the model of Lu *et al.* (2010) are also shown in Figure 3.3, which indicate that the SSCCs decrease as the temperature increases. The lower SSCC with increasing temperature indicates that the effective stress in the soil will decrease as the soil is heated. The properties of Bonny silt are summarized in Table 3.1

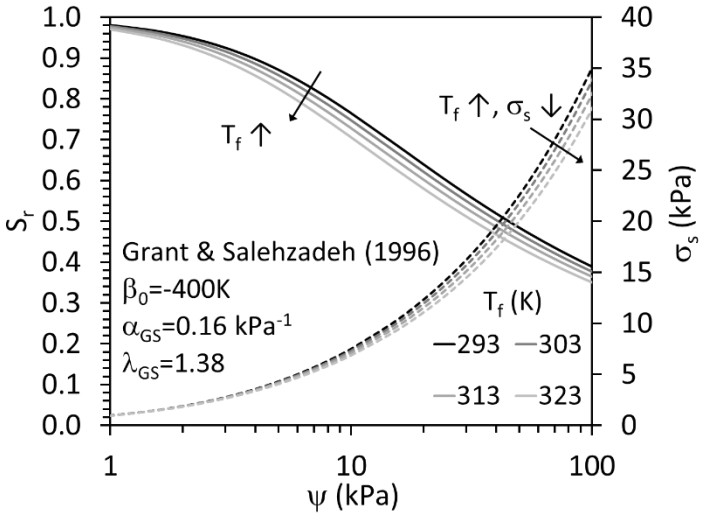

Figure 3.3 Drying path soil-water retention curve and suction stress characteristic curve for Bonny silt under different temperatures predicted using Grant and Salehzadeh (1996) and Lu *et al.* (2010), respectively

Table 3.1 Geotechnical properties of Bonny silt and initial conditions used in the experiments

Parameter	Value
D_{10}	<0.0013 mm
D_{30}	0.022 mm
D_{50}	0.039 mm
Liquid limit	25
Plastic limit	21
Plasticity index	4
Peak friction angle	34°
Initial target gravimetric water content	13.9%
Initial total density	1651.2 kg/m^3
Initial dry density	1450.0 kg/m^3
Initial void ratio	0.83
Initial porosity	0.45
Initial degree of saturation	0.44
Grant and Salehzadeh (1996) SWRC parameters	α_{GS} = 0.16 kPa^{-1} n_{GS} = 1.38 β_0 = -400K

Two geosynthetics were used in the testing program and their properties are given as the following. The first geosynthetic used in this study is a woven polypropylene (PP) geotextile manufactured by TenCate-Mirafi Inc. (product name Mirafi 600X). The PP geotextile has an ultimate tensile strength of 30.6 kN/m. The PP geotextile has a permittivity of 0.05 s^{-1} which indicates that is should not provide a significant barrier to water or gas flow during the heating process. The most important property governing the thermal response of a polymer is the glass transition temperature (T_g), defined as the temperature at which the polymer shows a reduction in tensile stiffness or ceases to behave as a brittle material. The PP geotextile has a glass transition temperature of -20 °C, which is lower than that of typical geothermal heat exchange applications of about 60 °C. It was observed, however, to have negligible effect on the stiffness of this geotextile.

The second geosynthetic used in this study is a woven polyethylene terephthalate (PET) geotextile manufactured by TenCate-Mirafi Inc. (product name Mirafi PET70/70). The PET geotextile has an ultimate tensile strength of 70 kN/m, and a creep-reduced tensile strength of 42 kN/m according to the manufacturer specifications. The PET geotextile has a permittivity of 0.1 s^{-1}. The PET geotextile has a glass transition value of 70 °C. It was assumed that the stiffness of the geotextile will remain constant for this study as they are below the glass transition value. An analysis of the magnitude of thermal softening on the tensile modulus for different geosynthetics was performed by Stewart *et al*. (2014a).

3.3 Experimental Procedures

The soil was prepared in 50 mm-thick lifts using dynamic compaction with an impact hammer. The soil was compacted directly on top of the heating coils on the bottom of the container, as shown in Figure 3.2(b). The dielectric sensors were placed at the interfaces between lifts, ensuring that the sensors were horizontal. The sensors were placed in such a manner that the cable would not provide any tensile resistance to the pullout. The sensor wires are routed to exit from the back of the container with a bend in the cable to again ensure that they do not provide tensile resistance during pullout testing. The sensors exit from a hole in the side of the container to avoid damage when applying the vertical stress. The interface between the layers were scarified to minimize the formation of weak zones within the layers. After compaction of the soil sample, the top surface was carefully leveled to ensure the top plate would apply a uniform stress to the soil along with applying a uniform boundary temperature. Negligible tilting was observed during compression and pullout, which indicated that relatively uniform stresses were applied through the entirety of the study. After the application of the vertical stress to the specimen 24 hours was

provided for consolidation to occur, this was sufficient to reach at least 90% of the consolidation settlement in all the tests.

For the first testing series, a uniform monotonic pullout was performed. The specimen was prepared and consolidated under a vertical stress of 19.5 kPa, which is representative of a soil element near the crest of a MSE wall as this is where pullout failure is most likely. At least 90% of primary consolidation occurred within 24 hours in all of the tests. After consolidation of the soil, the heating pump was turned on and set to the desired boundary condition temperature. The specimen was then monitored for 7 days to allow the soil to obtain as uniform of a temperature as possible while monitoring creep deformations. Next, the horizontal load was applied through a linear actuator at a constant rate of 0.0215 mm/min until pullout was achieved.

For the next testing series, the same vertical stress of 19.5 kPa was applied for 24 hours to consolidate the soil. After consolidation of the soil, however, the pulley-system was used to apply a seating pullout load of 1.43 kN/m (which corresponds to 10% of the peak pullout resistance in a room-temperature test, as will be noted) to the geosynthetic. The mechanical creep from this seating load was observed for 24 hours before turning on the heating pump to the desired boundary temperatures. Here the specimen was monitored for 7 days to allow the soil to again obtain as uniform of a temperature profile as possible while monitoring the thermal creep deformations. Next, the same constant displacement rate of 0.0215 mm/min was applied to the geosynthetic, and the pullout load was monitored until failure occurred.

Chapter 4

Results

4.1 Overview of Testing Program

The results of the two sets of pullout tests are presented in the following sections. It is worth noting that the values for volumetric water content obtained from the dielectric sensors used in this study were corrected for temperature effects using the model from Iezzoni and McCartney (2015). As these dielectric sensors typically show a spurious increase (or decrease) in volumetric water content, with different applied temperatures, the following correction was applied to accurately reflect changes caused by nonisothermal conditions.

$$\theta_w = A\epsilon_{actual} + B \ , \quad \text{where } \epsilon_{actual} = \epsilon_{measured} - \Delta T(m_{VWC} + m_d) \tag{4.1}$$

Here ε_{actual} is the dielectric permittivity of the soil without the temperature effect on the sensor, ΔT is the change in temperature, m_{VWC} and m_d are temperature correction slopes for the initial volumetric water content and initial dry densities respectively, and $\varepsilon_{measured}$ is the dielectric permittivity measured from the dielectric sensor corrected with Topp's equation, given as follows:

$$\epsilon_{measured} = 66.367\ \theta_{w,initial}^3 + 20.285\ \theta_{w,initial}^2 + 36.89\ \theta_{w,initial} + 1.891 \tag{4.2}$$

The initial soil conditions along with the differences in the geosynthetics used in each set of tests are summarized in Table 4.1. Both sets of tests were consolidated in the same manner, and under the same vertical applied pressure of 19.5 kPa. Consolidation data along with the application of the vertical stress for one of the test is shown in Figure 4.1. It was observed that the application

of the vertical stress did in fact cause the specimen to reach 90% consolidation within the 24 hour timeframe given for the consolidation phase. Additionally, very little tilting was observed when comparing the settlement measurements from both sides of the top plate thereby assuring that a uniformed pressure was applied. These observations of the consolidation phase remained the same throughout both testing series, so the remainder of the consolidation results are omitted.

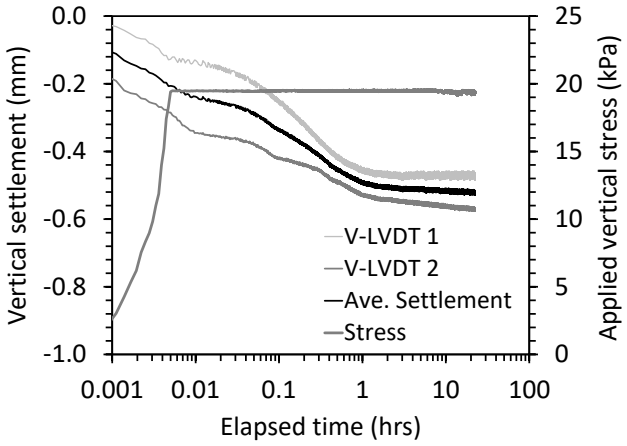

Figure 4.1 Typical consolidation data and applied vertical stress during the loading period of 24 hours

Table 4.1 Summary of initial soil conditions and geosynthetic specifications

Parameter	Monotonic Pullout after Heating without a Seating Load				Pullout with a Seating Load of 1.43 kN/m during Heating		
Initial void ratio, e_o	0.83	0.83	0.83	0.83	0.83	0.83	0.83
Initial degree of saturation, S_{r0}	0.44	0.43	0.43	0.44	0.43	0.43	0.46
Initial gravimetric water content, w_o (%)	13.89	13.57	13.43	13.87	13.81	13.69	14.65
Initial volumetric water content, θ_o (m^3/m^3)	20.14	19.67	19.48	20.12	20.06	19.89	21.28
Target temperature at the box boundaries, T_{target} (°C)	20	30	40	50	30	40	50
Geosynthetic	Mirafi 600X				PET 70/70		
Geosynthetic polymer	Polypropylene (PP)				Polyethylene terephthalate (PET)		
Ultimate tensile strength, T_{ult} (kN/m)	30.6				70		
Geotextile-silt pullout resistance at room temperature, P_{ult} (kN/m)	9.6				14.3		
Geotextile permittivity (s^{-1})	0.05				0.1		
Polymer glass transition temperature, T_g (°C)	-20				70		

The remainder of this chapter will focus on the results after the consolidation phase; that is for each testing series, results of both the heating phase and pullout phase will be discussed in greater detail along with the similarities, differences, and observations made for each testing series.

4.2 Testing Series 1 - Pullout Tests on PP Geotextiles

4.2.1 Heating Phase

The first set of tests results involved application of boundary temperatures ranging from 20 to 50 °C with an initial soil temperature of 23.4 °C. The change in temperature of the soil 13 mm below the soil-geosynthetic interface during the heating/cooling period are shown in Figure 4.2(a). The temperature of the soil was observed to increase (or decrease) rapidly, reaching steady state within a few days. The volumetric water contents (θ_w) were also recorded with the dielectric sensors and corrected for temperature effects, using the correction of Iezzoni and McCartney

(2015) model, and are shown in Figure 4.2(b). As expected, the heat from the heating coils causes drying of the silt, leading to a larger change in volumetric water content with higher temperatures. In general, more drying was observed closer to the heat exchangers at the top and bottom of the pullout box. The volumetric water contents required longer durations to reach steady-state than the temperatures.

The change in effective stress of the soil 13 mm below the soil-geosynthetic interface induced by the decrease in volumetric water content is shown in Figure 4.2(c). The effective stress was calculated using the effective saturation interpreted from the dielectric sensor measurements along with the suction interpreted using the SWRC model of Grant and Salahzadeh that accounts for the effects of temperature changes on the SWRC. An increase in effective stress of the soil 13 mm below the soil-geosynthetic interface was observed to increase for all four tests, with a greater increase in effective stress for greater changes in temperature. This increase in effective stress is expected to lead to both an increase in peak shear strength and an increase in stiffness. The change in vertical strain (i.e., void ratio) of the soil layer as a whole is shown in Figure 4.2(d). The measurement of vertical displacement was taken from the vertical LDVTs at the top of the pullout box thereby showing the change in vertical strain of the entire specimen and not simply the soil-geosynthetic interface. It can be observed that larger strains occur as the boundary temperatures are increased.

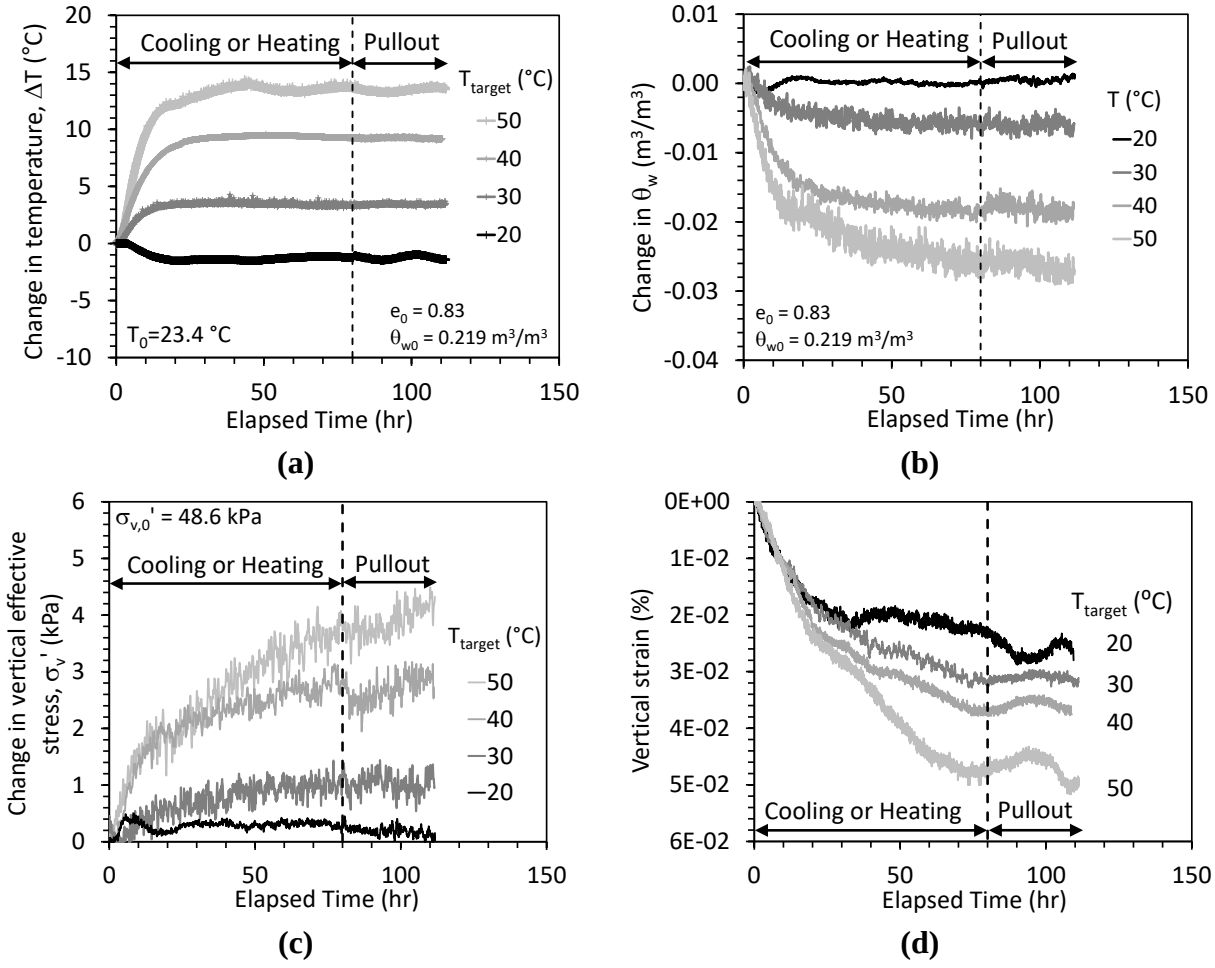

Figure 4.2 Thermo-hydraulic response of the soil for the specimens without a seating load: (a) change in temperature 13 mm below the soil-geosynthetic interface versus time; (b) change in volumetric water content 13 mm below the soil-geosynthetic interface versus time; (c) change in effective stress 13 mm below the soil-geosynthetic interface versus time; (d) change in vertical strain for the entire soil layer versus time

The temperature profiles at the end of the heating/cooling phase are shown in Figure 4.3(a). These measurements are taken directly from the dielectric sensors embedded in the soil and the thermocouples which are located near the heating coils. Both the topmost and bottommost temperature measurements are approximately equal to the targeted boundary temperatures confirming that the boundary temperatures were the same in this series of tests. The corresponding change in volumetric water content (i.e., from the start of heating to immediately before geotextile pullout) measured from the dielectric sensors and the actual volumetric water contents from physical sampling of the soil at the end of the testing are shown in Figures 4.3(b) and 4.3(c)

respectively. Note that the initial volumetric water contents before heating were approximately uniform and equal to 0.20. With an application of higher boundary temperatures, the volumetric water content of soil was observed to decrease relatively uniformly with height in the soil layer. This drying can be observed in the leftward shift of the volumetric water content profiles in Figures 4.3(b) and 4.3(c). It should be noted that the two sets of measurements are not identical as the sampling of the soil did not occur until after the specimen was disassembled, while the changes in volumetric water content from the dielectric sensors were immediately prior to pullout.

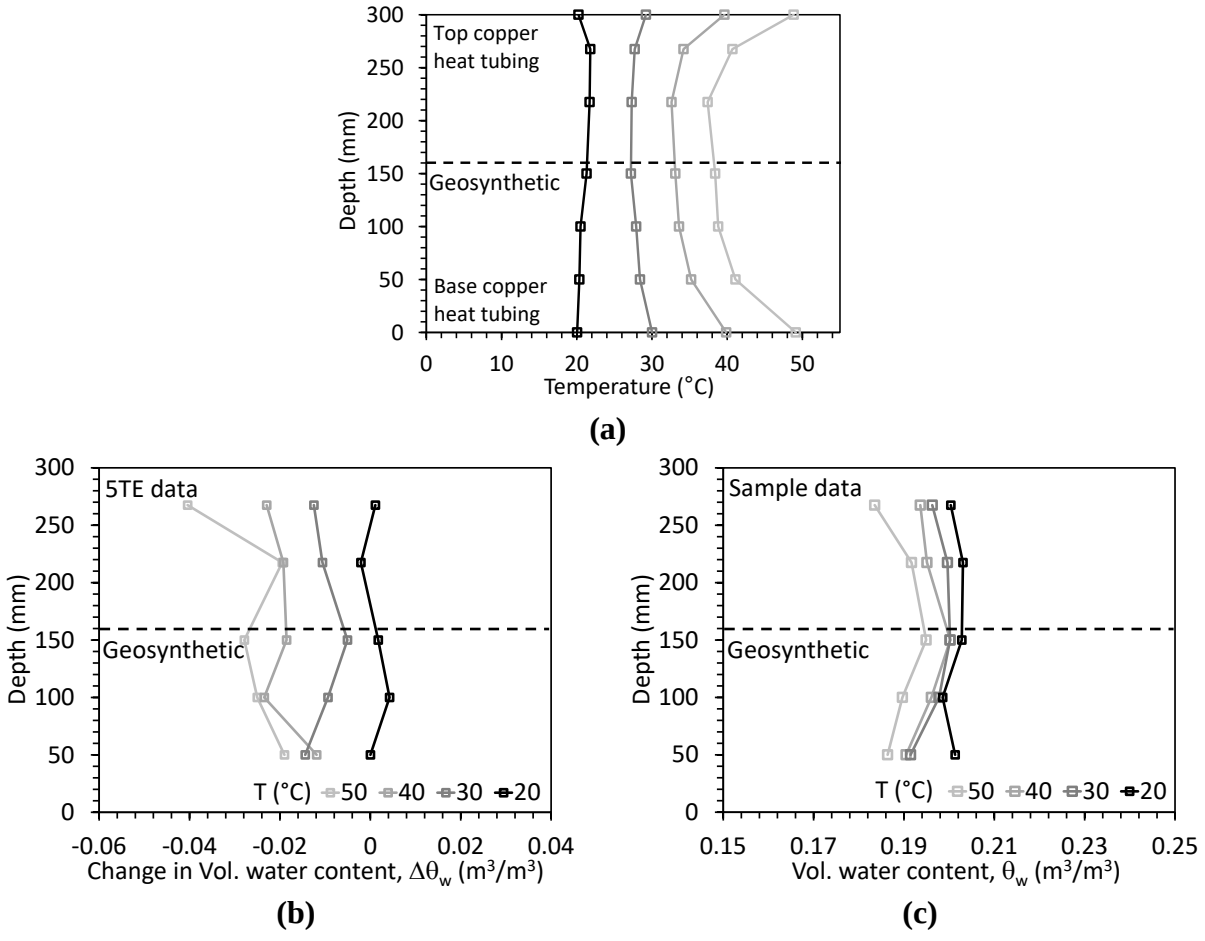

Figure 4.3 Monotonic pullout profile views of soil properties: (a) temperature distribution along the specimen; (b) change in volumetric water contents from dielectric from the start of heating phase to pullout; (c) average volumetric water content from sampling after test

4.2.2 Pullout Phase

Following the heating phase, the linear actuator was set at a constant displacement rate of 0.0215 mm/min and both the pullout load (from the horizontal load cell) and displacement (from the horizontal LDVT) were recorded versus time. These are combined in Figure 4.4(a) and show how the displacement follows a linear trend versus time while the pullout load varies in slope indicating that this is a displacement-controlled test. Alternatively, these figures can be combined to display the pullout force-displacement (P-d) curve which is shown in Figure 4.4(b). Several observations can be made from this P-d curve. Most importantly, as the boundary temperature increases the peak pullout force decreases. This can be attributed to the accumulation of water near the soil-geosynthetic interface (which will be further discussed in Chapter 5).

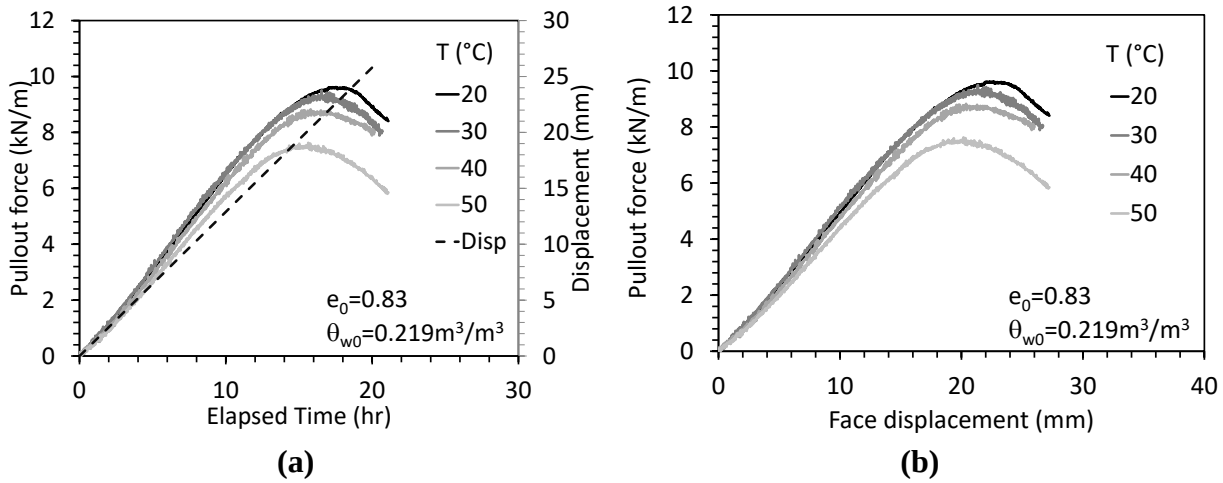

Figure 4.4 Monotonic pullout results: (a) Load versus time and displacement versus time; (b) force versus displacement (P-d) curve

4.3 Testing Series 2 - Pullout Tests on PET Geotextiles

4.3.1 Heating Phase

Prior to the start of the heating phase, a seating pullout load of 1.43 kN/m was placed on the PET geosynthetic which was given 24 hours for mechanical creep to occur before starting the

heating pump. This was implemented in order to isolate the thermal creep from the mechanical creep. The results for the thermal creep from the applied load are show in Figure 4.5. The applied seating load was equal to 10% of the ultimate pullout force that was observed from a monotonic room temperature test. The thermal creep in the tests in this testing series followed the proposed hypothesis from Stewart *et al.* (2013), where higher boundary temperatures resulted in greater thermal creep displacements. It is worth mentioning that the creep displacements from these tests were relatively insignificant compared to the displacement required to reach the ultimate pullout resistance (only about 5% of the peak displacement). The small creep displacement values are believed to be attributed to the distance of the geotextiles from the boundary heat sources. Since the heating coils were not on the same lift as the PET geosynthetic, the creep displacement is drastically lower than if the heating coils had been immediately above or below the soil-geosynthetic interface (i.e., on the same lift).

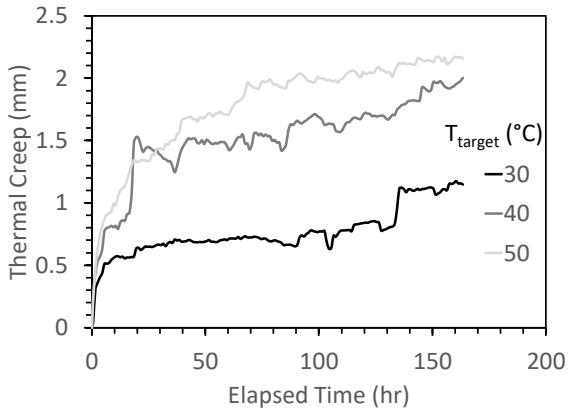

Figure 4.5 Thermal creep under a seating pullout load of 1.43 kN/m

During the heating phase, the thermo-hydraulic response of the soil layers were similar to those observed in the other testing series described in Figure 4.2, although only three boundary temperatures were analyzed in this set of tests (30, 40, and 50 °C). The soil temperature 13 mm below the soil-geotextile interface again reached steady state within a few days of starting the

heating pump, as shown in Figure 4.6(a). The change in volumetric water content versus time, shown in Figure 4.6(b), indicates that a decrease occurred in all three tests, although the tests at 40 and 50 °C showed an initial increase followed by a decrease. The magnitude of the change in volumetric water contents was slightly smaller in this testing series, which may be attributed to the fact that the boundary temperatures were not the same in all the tests, as will be noted below. An implication of the increasing and decreasing trend in volumetric water content in the tests at 40 and 50 °C is that the effective stress showed an initial decrease followed by an increase. However, the increase was not sufficient to lean to an overall increase in effective stress. It may be possible that the tests were not fully at steady-state. Nonetheless, it is also possible that the geotextile investigated in these tests did not act as a vapor drain leading to accumulation of water at the interface. This was investigated by using soil sampling to measure the volumetric water content directly at the soil-geosynthetic interface. The void ratio of the entire soil layer shown in Figure 4.6(d) indicates a slight contraction was observed in all the tests similar to the observation in the other testing series. However, no clear relationship between the change in void ratio and boundary temperature was observed in this testing series.

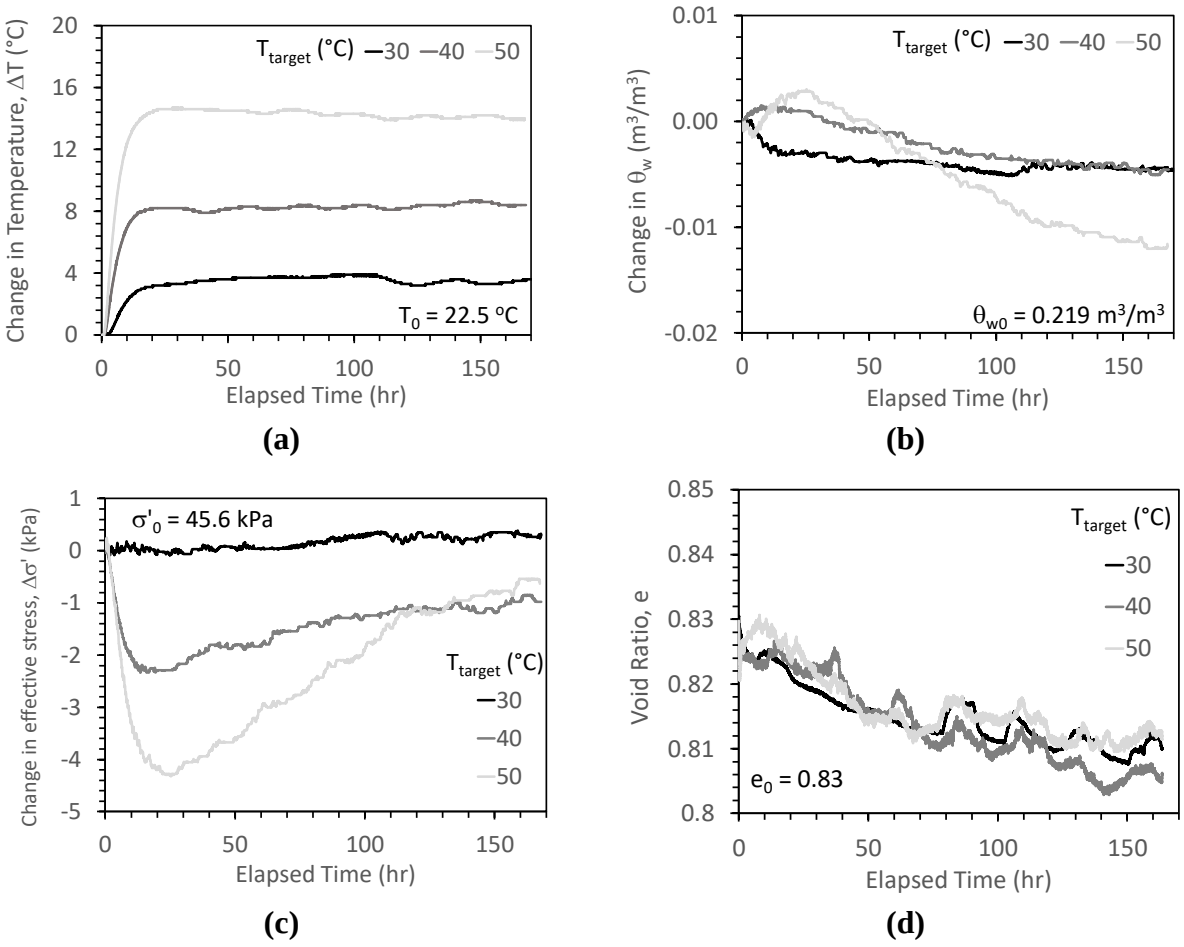

Figure 4.6 Thermo-hydraulic response of the soil for the specimens with a seating load: (a) change in temperature 13 mm below the soil-geotextile interface versus time; (b) change in volumetric water content 13 mm below the soil-geotextile interface versus time; (c) change in effective stress 13 mm below the soil-geotextile interface versus time; (d) void ratio for the entire soil layer versus time

The temperature profiles at the end of the heating phase are shown in Figure 4.7(a). It can be observed that there is a slight difference in boundary temperature in these experiments. Although the slightly hotter bottom boundary temperature may have led to more water vapor flow upwards toward the geosynthetic, it was only approximately 2-4 °C hotter. The change in volumetric water contents inferred from the dielectric sensors and the volumetric water content measured from soil samples are shown in Figures 4.7(b) and 4.7(c), respectively. Drying is observed in the lower part of the soil layer, but wetting is observed in the upper part of the soil layer. This may have occurred by water from the bottom of the soil layer evaporating and moving

towards the center but then condensing back in the upper portion of the soil-geosynthetic interface. The profiles of the actual volumetric water content from sampling shown in Figure 4.7(d) indicate a sharp break between the upper and lower parts of the soil-geosynthetic interface. This may indicate that water was condensing on the top part of the geotextile (i.e., on the bottom of the top half of the soil layer). Measurements of the volumetric water content directly at the soil-geosynthetic interface were not made in the pervious testing series, so the trends in the results in Figure 4.7(d) may also apply to the other testing series.

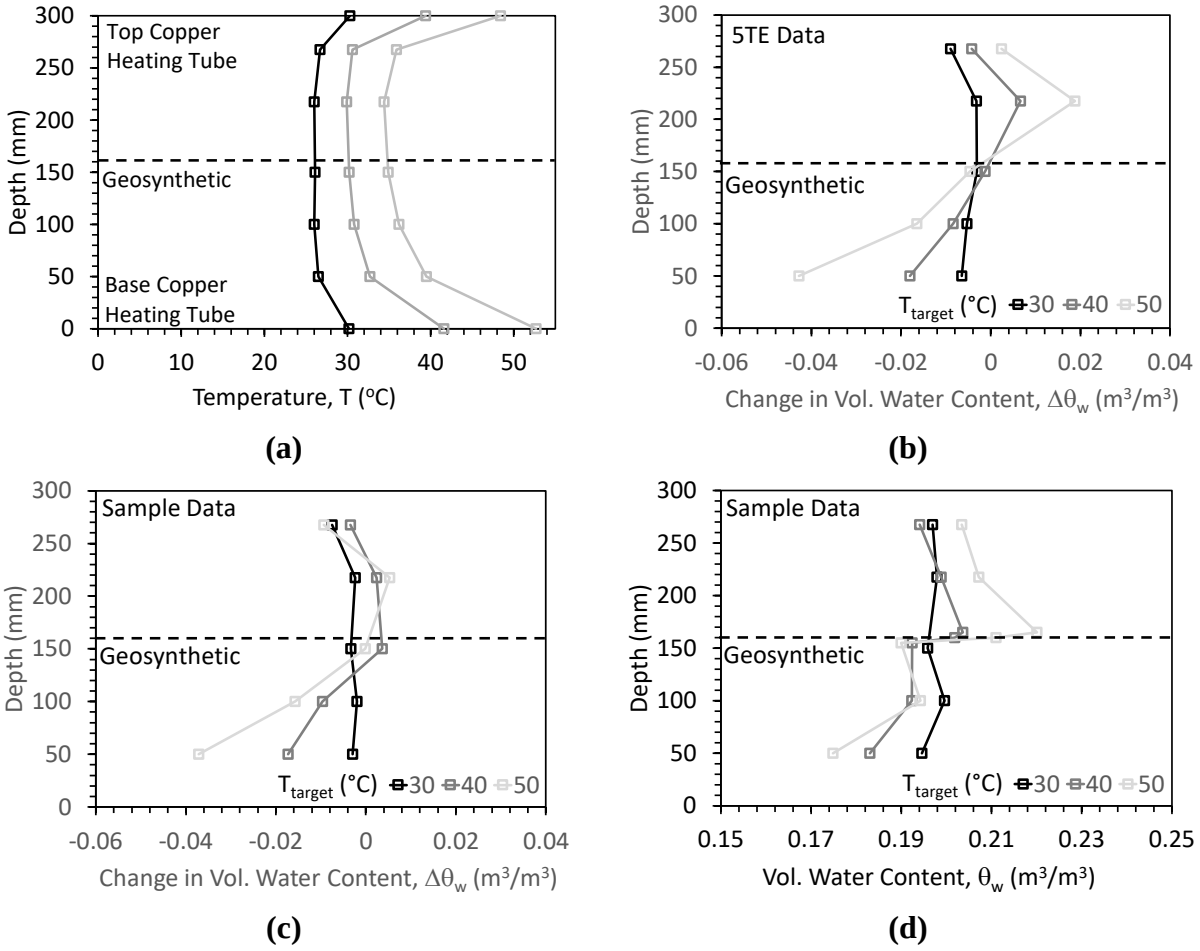

Figure 4.7 Seated load with monotonic pullout profile views of soil properties: (a) temperature distribution along the specimen; (b) change in volumetric water contents from dielectric sensors from the start of heating phase to pullout; (c) change in volumetric water contents from sampling from the start of construction to after completed test; (d) average post volumetric water content after each test

4.3.2 Pullout Phase

Prior to the presentation of the heating tests, two controlled room temperature tests were performed in order to determine an appropriate seating load. The first test was a monotonic room temperature test while the second test was a room temperature test with a seated load equal to 10% of the ultimate pullout resistance from the first test. These results are presented in Figure 4.8, and the seating pullout load of 1.43 kN/m was used for the remainder of the tests.

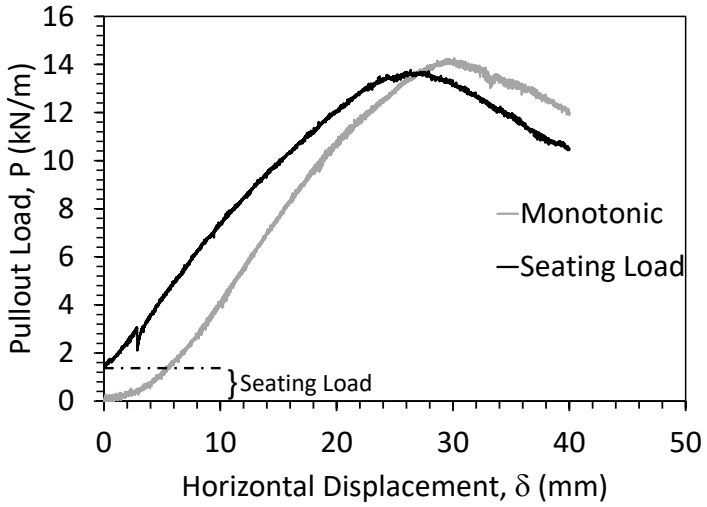

Figure 4.8 Room temperature pullout results for PET geotextile to determine seating pullout load

The displacements versus time along with the pullout force versus time are shown in Figure 4.9(a). Here the vertical shifts in the displacement curves exist because of the thermal creep that increases with increasing temperature. These vertical shifts correspond to horizontal offsets when plotting the force-displacement (P-d) curves, shown in Figure 4.9(b). Similar observations can be made between both series of tests; that is, an increase in boundary temperatures corresponds to a decrease in the pullout resistance.

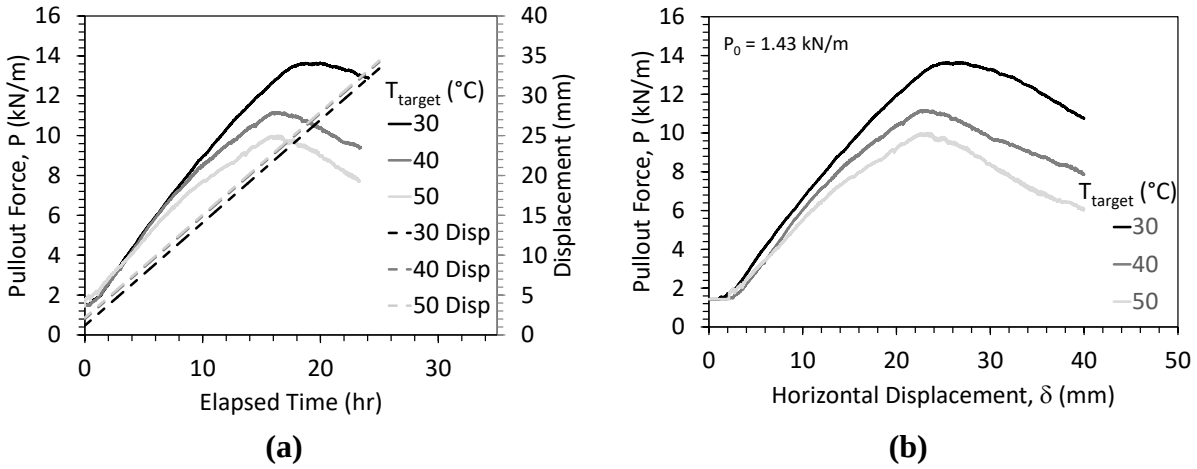

Figure 4.9 Seated load with monotonic pullout results: (a) load versus time and displacement versus time; (b) force versus displacement (P-d) curve

Chapter 5

Analysis

5.1 Synthesis of Experimental Results

To quantify the effects of temperature on the soil-geosynthetic interface of this study, the changes in temperature (i.e., heat transfer), volumetric water content (i.e., water flow), and changes in soil shear strength (i.e., the peak shear strength of the soil-geosynthetic interface) must be considered to interpret the different phenomena affecting the pullout resistance of geotextiles from unsaturated soil in nonisothermal conditions. When observing the results from both testing series, water tended to move from the heating coils to the center of the specimen. This is primarily due to the water within the specimen moving from regions of higher temperatures to lower temperatures. That is, as the water evaporated from the top and bottom of the soil box, leaving those areas dryer and stiffer after heating, the water vapor was then condensed near the center of the specimen, as shown in Figure 5.1, leaving that area softer and wetter. This primary hypothesis is supported by the post-test measurements of volumetric water content from soil sampling at the interface of the soil-geosynthetic interface in the pullout tests on the PET geotextile shown in Figure 4.7(d). After heating, the volumetric water content immediately above the soil-geosynthetic interface increased with increasing boundary temperature. The elevated boundary temperatures cause water to flow from the boundaries of the specimen toward the geotextile at the center. If the geotextile does not act as a vapor drain, then the water will condense at the top of the soil-geotextile interface.

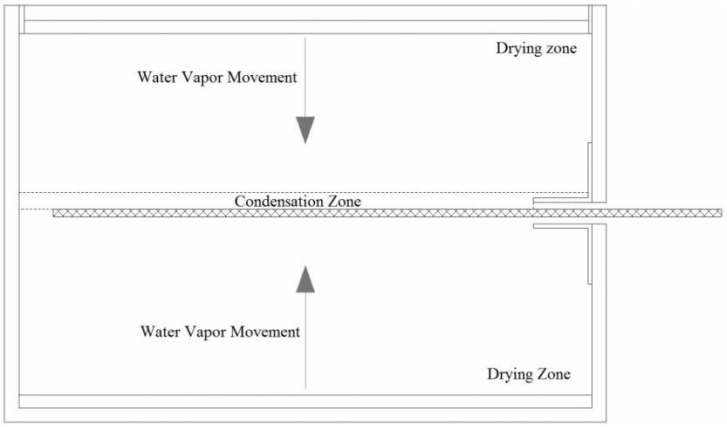

Figure 5.1 Hypothetical water movement within the specimen during the heating phase

From the results shown in figure 4.4(b) and Figure 4.9(b), the pullout resistance decreases with increasing boundary temperature. Specifically, decreases in pullout resistance of 20% and 30% were observed from the PP geosynthetic testing series and the PET geosynthetic testing series respectively. Based on the explanation of Figure 5.1, it is proposed that this increase in volumetric water content immediately at the soil-geosynthetic interface was the primary cause of the decrease in the pullout resistance with increasing boundary temperature observed for both geotextiles. When there is an increase in volumetric water content at a given location in the soil layer, the suction stress will decrease leading to a decrease in effective stress.

5.2 Effective Stress Analysis of Pullout Resistance

The pullout resistance of a geotextile from a soil layer can be predicted using the following effective stress-based equation (Berg *et al.* 2009):

$$P_r = C\ \sigma_v'\ F^*\ L_e\ \alpha \qquad (5.1)$$

where C is a reinforcement effective unit parameter (typically equal to 2 for geotextiles as it has upper and lower interfaces with the soil), σ_v' is the vertical effective stress at the level of the geotextile, F* is the pullout resistance factor (defined here as F* = tan(ϕ), where ϕ is the drained

friction angle of the backfill soil), L_e is the embedment length (or in a MSE wall the length of geotextile in the resisting zone behind a failure surface), and α is a scale factor to account for a non-linear stress reduction over the embedded length of highly extensible reinforcements (typically 0.6 for geosynthetic reinforcements) (Berg *et al.* 2009). This equation can be applied directly to infer the effects of unsaturated conditions on geosynthetic pullout by incorporating the definition of vertical effective stress in unsaturated soils (Equation 2.1). The effective saturation used in the definition of the vertical effective stress should be the value in the soil at the soil-geosynthetic interface (and perhaps the average value of the effective saturation in the soil above and below the geotextile in case they are different).

When applying Equation 2.1 to soil layers under nonisothermal conditions such as those evaluated in this study, it may be possible to use the effective saturation directly at the soil-geosynthetic interface, which indirectly incorporates the effects of thermally-induced water flow in the unsaturated backfill soil. However, it may also be possible that thermal softening of the soil such as that observed by Uchaipichat and Khalili (2009) plays a role as well. The trends in the peak shear strength as a function of temperature for three suction values interpreted from the stress-strain curves of Uchaipichat and Khalili (2009) are shown in Figure 5.2. A thermal softening parameter μ is also shown for each set of tests at the same matric suction, defined as the percent change in peak shear strength as a function of temperature (units of %/°C). The results in Figure indicate that suction does not have a significant effect of the value of μ, so a value of $\mu = 0.002$ was used in this study.

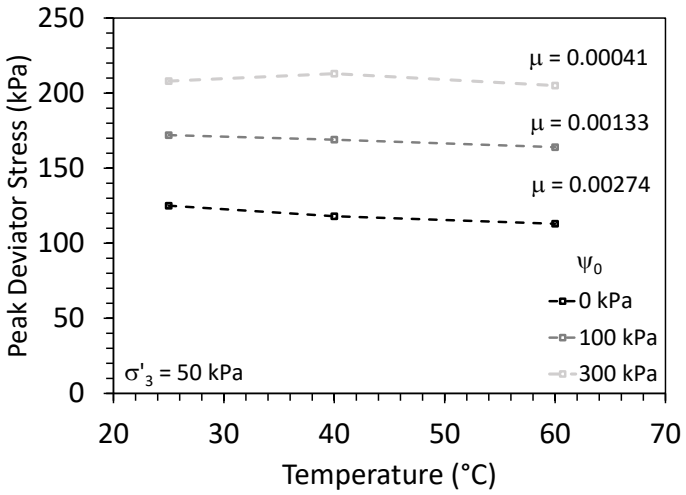

Figure 5.2 Definition of the thermal softening parameter from the temperature- and suction-controlled triaxial compression shear tests of Uchaipichat and Khalili (2009)

The equation for pullout resistance can then be modified to account for thermal softening, as follows:

$$P_r = C\ \sigma'_v\ F^*\ L_e\ \alpha\ \left(1 - (\mu\ \Delta T)\right) \tag{5.2}$$

where ΔT is the change in temperature at the soil-geosynthetic interface. The negative sign in the brackets indicates that a change in temperature will lead to a decrease in the pullout resistance due to the effect of thermal softening.

Equations 5.1 and 5.2 were used to predict the pullout resistance of the PP geotextile from compacted silt, as shown in Figure 5.3(a) and 5.3(b) with the pullout resistance plotted as a function of temperature and effective stress, respectively. Although a good match is observed for low changes in temperature, a significant divergence is observed for higher changes in temperature (where both equations predict an increase in pullout resistance). This is due to the effective saturation values at the time of pullout for these tests were interpreted from the dielectric sensor 13 mm below the soil-geosynthetic interface, rather than directly at the soil-geosynthetic interface.

It is possible that the soil on top of the soil-geosynthetic interface experienced an increase in volumetric water content as hypothesized in Figure 5.1. Since sampling of the soil at the interface after pullout was not performed for this set of tests, this cannot be confirmed.

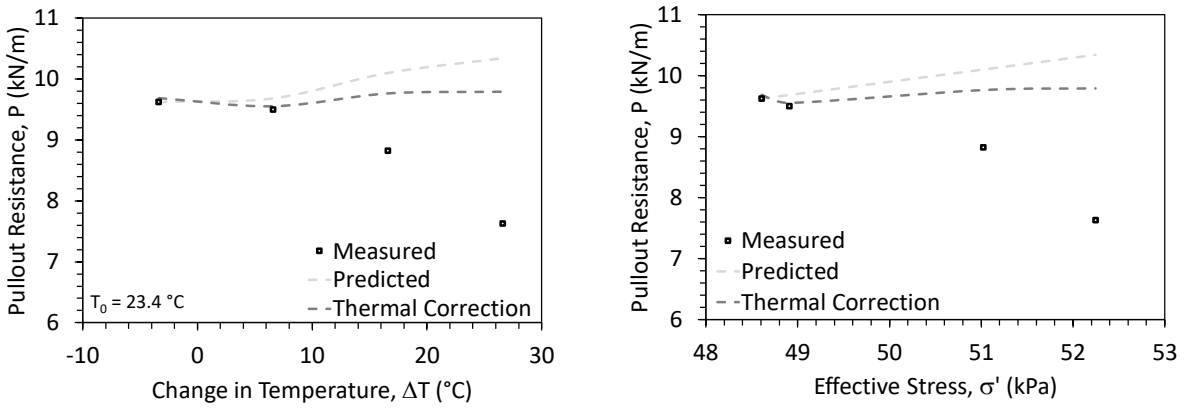

(a) **(b)**

Figure 5.3 Comparison of the measured and predicted pullout resistances for the tests on PP geotextiles without a seating pullout load: (a) pullout resistance versus temperature; (b) pullout resistance versus effective stress

Equations 5.1 and 5.2 were used to predict the pullout resistance for the tests on the PET geotextiles in compacted silts, as shown in Figures 5.4(a) and 5.4(b) with the pullout resistance plotted as a function of temperature and effective stress, respectively. In this case, because the effective saturation on the top side of the soil-geosynthetic interface was used in the analysis, a very good match between both equations and the measured pullout resistances is observed. The incorporation of the thermal softening parameter in Equation 5.2 does not lead to a significant improvement in the prediction of the pullout resistance. This is likely because the positive effects of suction on the peak shear strength are greater than the negative effects of temperature on the pullout resistance.

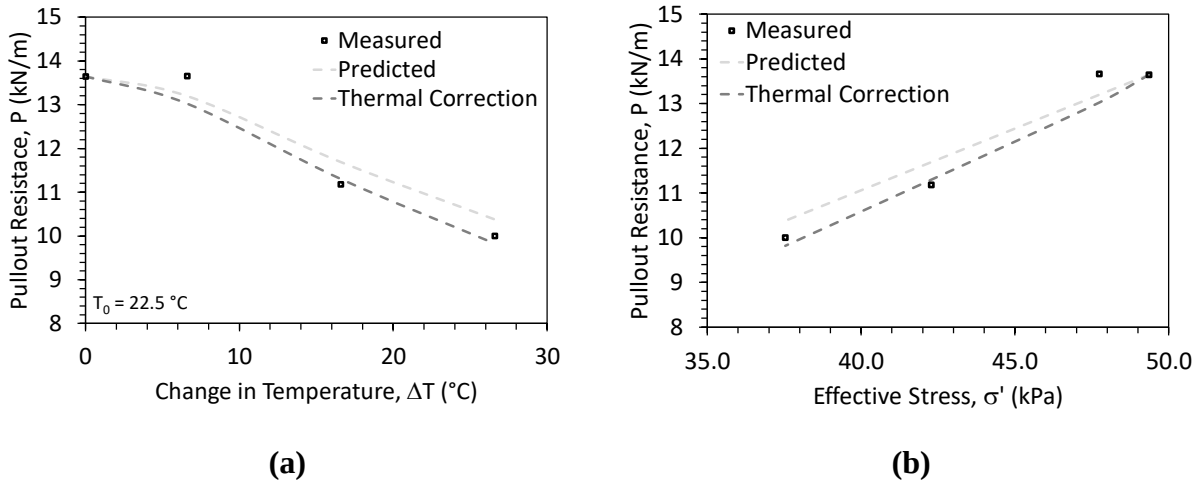

Figure 5.4 Comparison of the measured and predicted pullout resistances for the tests on PET geotextiles with a seating pullout load: (a) pullout resistance versus temperature; (b) pullout resistance versus effective stress

The prediction results from the tests on the PET geotextile reinforces the hypothesis that when temperature is applied at the boundaries (i.e., top and bottom of the soil box) the pullout force will decrease as water from thermally induced drying of the soil layer will tend to accumulate at the soil-geosynthetic interface. It the geotextile reinforcements act as a good vapor drain, then the predicted pullout resistances from Equations 5.1 and 5.2 indicate that the soil should be getting stronger with a higher boundary temperature. Further, if heating elements were placed at the same location as the geosynthetic, the direction of thermally-induced water flow will be away from the geosynthetic reinforcement.

Although the prediction does not accurately predict the pullout resistance in the tests on PP geotextile, it does give insight to how geothermal heat sinks can be used to ultimately increase the pullout resistance of poorly draining backfill in an MSE wall so long as the change in effective stress is positive (i.e, water moves away or is removed from the soil-geosynthetic interface). Table 5.1 summarizes the percent error between the two models of the pullout force prediction for each corresponding geotextile.

Table 5.1 Percent errors between measured and prediction models of pullout resistances for PP and PET geotextiles

Boundary Temperatures (°C)	PP Prediction (%)	PP Thermal Correction (%)	PET Prediction (%)	PET Thermal Correction (%)
20.0	0*	0*	N/A	
22.5	N/A		0*	0*
30.0	1.9	0.6	3.4	4.7
40.0	14.5	10.7	4.5	1.0
50.0	35.6	28.4	3.8	1.7

Note: "*" Depicts the reference temperature for the prediction model and therefore no percent error exists.

Chapter 6

Conclusion

6.1 Conclusion

This study involved the investigation of the effects of temperature on the interaction mechanisms between reinforcing geotextiles confined in unsaturated, compacted silt. The testing procedure developed in this study analyzed the pullout resistance of two different geotextiles (polypropylene and polyethylene-terephthalate) under different loading conditions (with and without a seating pullout load, respectively) as well as boundary temperatures ranging from 20 to 50 °C. The first set of tests involved monotonic pullout of a PP geotextile after reaching steady-state thermo-hydraulic conditions without a seating pullout load, while the second set of tests involved a monotonic pullout on a PET geotextile after reaching steady-state thermo-hydraulic conditions while under a seating pullout load.

The results from the two testing series indicate that the ultimate pullout resistance of the geotextiles heated with and without a seating pullout load decreased with increasing boundary temperature. It was found that heating lead to nearly uniform drying of the silt layer although water was observed to accumulate at the soil-geotextile interface leading to a decrease in ultimate pullout resistance. An effective stress analysis was performed on the resulting pullout resistances to analyze the thermal softening mechanisms in the silt. A good match was observed between the predicted and measured pullout resistances as long as the effective saturation at the soil-geosynthetic interface was used in the analysis. A model considering thermal softening trends

obtained from the nonisothermal stress-strain curves of silt measured by Uchaipichat and Khalili (2009) was not found to provide a significant change in the prediction of the pullout capacity of geotextiles from compacted layers with increasing boundary temperatures. This indicates that a good understanding of the thermo-hydraulic conditions at the soil-geosynthetic interface may be sufficient to accurately predict the pullout resistance.

6.2 Recommendations for Future Research

Although this study found that elevated temperatures may have a detrimental effect on the soil-geosynthetic interaction in MSE walls, it is possible that an improvement in behavior would be observed if the geothermal heat exchangers were installed at the same locations as the geosynthetic reinforcements. This alternative can be performed using the same pullout device. One shortcoming of such an approach is that the temperature at the geosynthetic would be greater and there would be more possibility for thermally induced creep. However, the amount of creep displacement observed in this study was not significant. The impact of different temperatures and different magnitudes of seating pullout load do need to be considered however. Future studies should ensure that the volumetric water content of the soil directly at the soil-geosynthetic interface is monitored, preferably at the top and bottom of the geosynthetic. An investigation into different types of geotextiles that may have wicking capabilities should be performed, as these may be able to remove the water that accumulates at the soil-geosynthetic interface. Use of wicking geotextiles may add flexibility in where the geothermal heat exchangers are located within the MSE wall and they may promote more uniform thermally-induced drying.

References

Alsherif, N.A. and McCartney, J.S. (2015). “Nonisothermal behavior of compacted silt at low degrees of saturation.” *Géotechnique*. 65(9), 703-716.

Alsherif, N. and McCartney, J.S. (2016). “Yielding of silt at high temperature and suction magnitudes.” *Geotechnical and Geological Engineering*. 34(2), 501-514.

Berg, R.R., Christopher, B.R., and Samtani, N.C. (2009). Design and construction of mechanically-stabilized earth walls and reinforced soil slopes – Volume I. *FHWA-NHI-10-024*, FHWA, U.S. Department of Transportation, Washington, D.C., USA.

Bishop, A.W. (1959). “The principle of effective stress.” *Teknisk Ukeblad I Samarbeide Med Teknikk*, Oslo, Norway, 106(39), 859-863.

Bolzon, G., Schrefler, B.A., and Zienkiewicz, O.C. (1996). “Elastoplastic soil constitutive laws generalized to partially saturated states.” *Géotechnique*. 46(2), 279-289.

Brand, S.R., and Duffy, D.M. (1987). "Strength and pullout testing of geogrids." *Geosynthetics' 87*, 226-236.

Bueno, B.S., Costanzi, M.A. and Zornberg, J.G. (2005). “Conventional and accelerated creep tests on nonwoven needle punched geotextiles.” *Geosynthetics International*. 12(6): 276-287.

Campanella, R.G. and Mitchell, J.K. (1968). “Influence of temperature variations on soil behavior.” American Society of Civil Engineers Proceedings. 94(SM3), 709-734.

Carpenter, D., Zhang, M., Stewart, M.A. and McCartney, J.S. (2015). “Pullout Device for Nonisothermal Response of Reinforcing Geosynthetics in Thermally-active Geotechnical Systems.” Geosynthetics 2015. Portland, OR. Feb. 15-18. 1-9.

Cekerevac, C. & Laloui., L. 2004. “Experimental study of the thermal effects on the mechanical behavior of a clay”. *International Journal of Numerical and Analytical Methods in Geomechanics*, 28, 209–228.

Chang, D.T.T., Chang, F.C., Yang, G.S., and Yan, C.Y. (2000). “The influence factors study for geogrid pullout test.” *Grips, Clamps, Clamping Techniques, and Strain Measurement for Testing of Geosynthetics, ASTM STP 1379*. 129-142.

Coccia, C.J.R. and McCartney, J.S. (2013). “Impact of heat exchange on the thermo-hydro-mechanical response of reinforced embankments.” Proceedings of GeoCongress 2013. ASCE. San Diego, CA. Mar. 3-5. 343-352.

Coccia, C.J.R. and McCartney, J.S. (2016a). “Thermal volume change of poorly draining soils I: Critical assessment of volume change mechanisms.” Computers and Geotechnics. 80(December), 26-40.

Coccia, C.J.R. and McCartney, J.S. (2016b). “Thermal volume change of poorly draining soils II: Constitutive modelling.” Computers and Geotechnics. 80(December), 16-25.

Farrag, K., Acar, Y.B., and Juran, I. (1993). "Pull-out resistance of geogrid reinforcements." *Geotextiles and Geomembranes.* 12(2), 133-159.

Grant, S. A., and A. Salehzadeh (1996), “Calculation of temperature effects on wetting coefficients of porous solids and their capillary pressure functions”, *Water Resource Research*, 32(2), 261–270.

Hueckel, T., and G. Baldi (1990). “Thermoplasticity of Saturated Clays: Experimental Constitutive Study.” *Journal of Geotechnical Engineering*, 116(12), 1778–1796.

Karademir, T. (2011). Elevated Temperature Effects on Interface Shear Behavior. Doctoral Dissertation. GaTech, Atlanta, GA.

Khalili, N., Geiser, F. & Blight, G. E. (2004). “Effective stress in unsaturated soils: a review with new evidence”. Int. J. Geomech. ASCE 4, No. 2, 115–126

Khosravi, A. and McCartney, J.S. (2012). “Impact of Hydraulic Hysteresis on the Small-Strain Shear Modulus of Unsaturated Soils.” *ASCE Journal of Geotechnical and Geoenvironmental Engineering*. 138(11), 1326–1333.

Khosravi, A., Alsherif, N., Lynch, C., and McCartney, J.S. (2012). “Use of multistage triaxial testing to define effective stress relationships for unsaturated soils.” *ASTM Geotechnical Testing Journal*. 35(1), 128-134.

Lu, N., and W. J. Likos (2006), “Suction stress characteristic curve for unsaturated soil”, *Journal of Geotechnical and Geoenvironmental Engineering*, 132(2), 131–142.

Lu, N., Godt, J.W. and Wu, D.T. (2010). “A closed-form equation for effective stress in unsaturated soil.” *Water Resources Research*. 46: 1-14.

McGown, A., Andrawes, K. Z. and Kabir, M. H. (1982), “Load-Extension Testing of Geotextiles Confined in Soil.” Proceedings of the Second International Conference on Geosynthetics, Vol. 3, IFAI, Las Vegas, Nevada, USA, August 1982, 793-798.

Philip, J. R., and D. A. De Vries (1957), “Moisture movement in porous materials under temperature gradients”, *Eos Trans. AGU*, 38(2), 222–232.

Saix, C., Devillers, P. & El Youssoufi, M. S. (2000). “Thermomechanical coupling elements in the consolidation of unsaturated soils”. Canadian Geotechnical Journal. 37, 308-317.

She, Hugh Y., and Brent E. Sleep (1998). “The Effect of Temperature on Capillary Pressure-Saturation Relationships for Air-Water and Perchloroethylene-Water Systems.” *Water Resources Research*, 34(10), 2587–2597.

Stewart, M.A. and McCartney, J.S. (2013). "An Analytical Model for Predicting Lateral Face Deflections of Thermally Active Mechanically Stabilized Earth Walls." International Symposium on Design and Practice of Geosynthetic-Reinforced Soil Structures. H.I. Ling, G. Gottardi, D. Cazzuffi, J. Han, F. Tatsuoka, eds. DEStech Publications. 233-242.

Stewart, M.A., Coccia, C.J.R., and McCartney, J.S. (2014a). "Issues in the Implementation of Sustainable Heat Exchange Technologies in Reinforced, Unsaturated Soil Structures." Proceedings of GeoCongress 2014 (GSP 234), M. Abu-Farsakh and L. Hoyos, eds. ASCE. 4066-4075.

Stewart, M.A., Coccia, C.J.R., and McCartney J.S. (2014b). "Physical Modeling of the Thermal-Hydro-Mechanical Response of a Thermally Active Soil-Geosynthetic System. Proceedings of the 10th International Conference on Geosynthetics (ICG 10). Berlin, Germany. Sep. 21-25. 1-10.

Sun, D., Sun, W., and Xiang L. (2010). "Effect of Degree of Saturation on Mechanical Behavior of Unsaturated Soils and Its Elastoplastic Simulation." *Computers and Geotechnics*. 37(5), 678–688.

Thomas, H.R., He, Y., Sansom, M.R. and Li, C.L.W. (1996). "On the development of a model of the thermo-mechanical-hydraulic behavior of unsaturated soils." *Engineering Geology*. 41, 197-218.

Uchaipichat, A. and Khalili, N. (2009). "Experimental investigation of thermo-hydro-mechanical behavior of an unsaturated silt." *Géotechnique*. 59(4), 339-353.

van Genuchten, M. T. (1980), "A closed-form equation for predicting the hydraulic conductivity of unsaturated soils", *Soil Science Society of America Journal*, 44, 892–898.

Vega, A. and McCartney, J.S. (2015). "Cyclic heating effects on thermal volume change of silt." *Environmental Geotechnics*. 2(5), 257-268.

Zornberg, J.G. and Mitchell, J.K. (1994). "Reinforced soil structures with poorly draining backfills. Part I: Reinforcement interactions and functions." *Geosynthetics International*. 1(2): 103-148.

Zornberg, J.G., Christopher, B.R. and Mitchell, J.K. (1995). "Performance of a geotextile-reinforced slope using decomposed granite as backfill material." Proc. of the 2nd Brazilian Symposium on Geosynthetics. São Paulo, Brazil. 19-29.

Zornberg, J.G., Byler, B.R. and Knudsen, J. (2004). "Creep of geotextiles using time-temperature superposition methods." JGGE. 130(11): 1158-1168.